Investigation of Sulphur Based Passivation Treatments of III-IV Semiconductor Surfaces

By B.M. Murphy, BSc.

Supervisor: Dr. Greg Hughes.

Submitted for the Degree of Master of Science
September 1994.

List Of Contents

Acknowledgements

I would like to thank my supervisor Dr. Greg Hughes for all his help and encouragement with this work and for his limitless patience with me. A special word of thanks too to Dr. Tony Cafolla for all his help and humour and thanks to both station masters at Daresbury, David Teehan and Dr. Paul Bailey for all their help at Daresbury. Thanks too to Dr. Dave Woolf of University Colledge Cardiff, Wales for providing the As capped GaAs(111) samples. I would also like to thank Eolas Strategic Research Programme for funding this project (and Boris!!).

I would like to thank the postgrads at D.C.U. for their friendship and support over the years especially the coffee gang for their meaningful insights on life and physics! I'd also like to thank the all lecturers, past and present, and technical staff who often went out of their way to help me, also Marion and Jackie for cheering up many days.

To my parents, John and Cecilia, I'd like to say I can never thank you both enough for all the help, and support you've given me, and for all the baby sitting!!!! To all my other baby-sitters John, Barry (thanks brov's), Both Nanas, Kathleen, Breda, Vera, Ruth, Tina, Mary, Brid, Marie, Oonagh, Mick, Margaret, Helen, Emer and all the Doyles, Josephine, the Lithgows and everyone else there at the drop of a hat, thank you. I am indebted to Lynn and all the girls at the Crèche at D.C.U. and to D.C.U. students union for helping to meet the bills. Finally a most special thank you to Dave and Joseph without whom all this would be meaningless.

Declaration

I hereby certify that this material, which I now submit for assessment on the programme of study leading to the award of Masters Degree is entirely my own work and has not been taken from the work of others save and to the extent that such work has been cited and acknowledged within the text of my work

Signed: Bridget Murphy Date: 16/2/95

Candidate

Abstract

The electronic and chemical properties of GaAs(111) Surfaces have been investigated at Daresbury Synchrotron Radiation Source in Ultra High Vacuum (UHV) conditions before and after molecular sulphur adsorption. The surface geometry has been determined using Low Energy Electron Diffraction (LEED). The surface composition and electronic structure have been studied using angle integrated and angle resolved photoemission. The objective was to gain an understanding of the chemical and electronic passivation mechanisms resulting from the termination of the GaAs(111) surfaces by a sulphur monolayer. The results indicate that these systems are complex with evidence of surface and substrate interactions.

Passivation work on InP was carried out at Dublin City University. InP samples which had been chemically etched, plasma etched and treated with molecular sulphur have been compared. Simple Schottky barrier devices were fabricated in UHV conditions. The device characteristics were then determined using current-voltage and capacitance-voltage profiles and deep level transient spectroscopy. There are indications that this surface treatment may well prove to have practical applications in device fabrication.

Chapter 1 General Introduction

1.1 Surface Physics

Surface physics is the study of the chemical composition and atomic structure at the surfaces of solids and the theory and observation of their structural, electronic, and chemical properties. The surface of any material will differ from the bulk in that the surface atoms have a lower co-ordination number. The atoms at the surface of a material may rearrange to take account of their local bonding arrangement giving rise to a surface reconstruction. Either way the electronic and chemical properties of the surface are generally significantly different from those of the bulk.

The interfaces between the different materials used in device fabrication can have a major influence on how the device functions. Therefore to understand the device it is necessary to know the electronic and chemical properties of the surface as well as the bulk. Device performance is often affected by the existence of surface states and also by surface oxidation. In order to improve device performance the work for this project has been an attempt to chemically and electronically passivate the surface of III-V semiconductors. By chemical passivation, the surface is made more resistant to ambient oxidation and by electronic passivation band gap states near the surface i.e. surface states are removed or reduced.

The study of III-V semiconductors has been driven by their device applications. Both GaAs and InP have wide band gaps and have applications as optical devices. A wide range of surface science techniques has been applied to study the microscopic interactions and Schottky barrier formation for metals and other overlayers deposited on clean and oxide-covered III-V semiconductors. As part of this project the electronic properties of Schottky diodes were investigated using current-voltage (I-V), capacitance voltage (C-V) and deep level transient spectroscopy (DLTS) techniques . Surface studies were carried out in ultra high vacuum (UHV) conditions using low energy electron diffraction (LEED), Auger electron spectroscopy and photoemission techniques. These techniques will be discussed in chapter 2. The overall aim of the project is to investigate the passivating effects of sulphur a group VI element on InP and GaAs; both III-V semiconductors. Chemical passivation means the production of a surface which is to a large extent chemically inert while electronic passivation results in the removal of surface states introduced into the band gap of the

semiconductor by surface reconstruction or oxidation. The following chapters give details of the attempts to chemically and electronically passivate the surfaces of III-V semiconductors. The termination of the surfaces of III-V semiconductors by a monolayer of sulphur has been proposed as a method of simultaneously achieving these two complementary properties. Two different passivation techniques are employed. Chapter 3 discusses wet chemical sulphur passivation of InP(100) surfaces, Chapters 4 and 5 describe photoemission studies molecular sulphur passivation of GaAs(111) and Chapter 6 contains the conclusions and suggestions for future work.

1.2 Indium Phosphide

Due to the high electron mobility and wide band gap of InP (1.4 eV) it has many device applications [1]. These include high speed devices, microwave devices, high power switching devices and optical devices. InP is reported as being a suitable material for solar cells because it has excellent radiation resistance characteristics. Williams, Varma and Montgomery (1979) and Spicer *et al.* (1980) [2,3] concluded that most metal-InP interfaces are non abrupt and disordered, with a high density of defects which would be capable of pinning the fermi level at the interface. The work in this thesis includes investigating the passivating effects of wet chemical etches on the InP surface before putting down a metal overlayer.

1.3 Gallium Arsenide

There have been many studies of the various GaAs surface reconstructions. The GaAs(110) surface is probable the most researched surface due to the fact that it can be obtained by cleaving. Investigations have shown that there are no surface states in the bulk band gap for clean, well ordered surfaces [4]. The GaAs (100) surface has also been the subject of many investigations of it's different surface reconstructions, by LEED, Auger, scanning tunnelling microscopy (STM) and photoemission studies. A recent study investigated the passivating effects of sulphur on this surface [5]. In this thesis it is the GaAs(111) surfaces that have been investigated using both core level photoemission and angle resolved photoelectron spectroscopy and also LEED and Auger spectroscopy. Both the clean and sulphur terminated surfaces are investigated.

References.

[1] M. Glicksman, K Weiser, J. Phys. Chem. Solids (UK) **10**(1959) p.337-340.

[2] R.H. Williams, R.R. Varma and V. Montgomery, J. Vac. Sci. Technol. **21** (1979) p.1418.

[3] W.E. Spicer, I. Lindau, P. Skeath and C.Y. Su, J. Vac. Sci. Technol. **17** (1980) p.1019.

[4] G.V. Hanson and R.I.G. Uhrberg, Surf. Sci. Rep. **9** (1988) p.197.

[5] P. Morioraty, B. Murphy, L. Roberts, A.A. Cafolla, G. Hughes, L. Koenders and P. Bailey, accepted for pub. by Surf. Sci..

Chapter 2 Experimental Techniques.

2.1 Introduction.

This chapter give a brief description of the theory behind the experimental techniques used in this work.

2.2 Electrical Techniques.

2.2.1 I-V and C-V Measurements.

In order to discuss the current-voltage (I-V) and capacitance-voltage (C-V) measurements let us look at a Schottky barrier. When a metal comes in contact with an n-type semiconductor electrons flow from the semiconductor to the metal until the two Fermi levels equalise, and so a potential barrier is formed (see figure 2.1) The rectifying properties of the Schottky Barrier [1] are determined by the height of this potential barrier $\phi_B = \phi_m - \chi_s$. This barrier height may be determined by measuring the current through the device or the capacitance of the device with respect to an applied bias voltage.

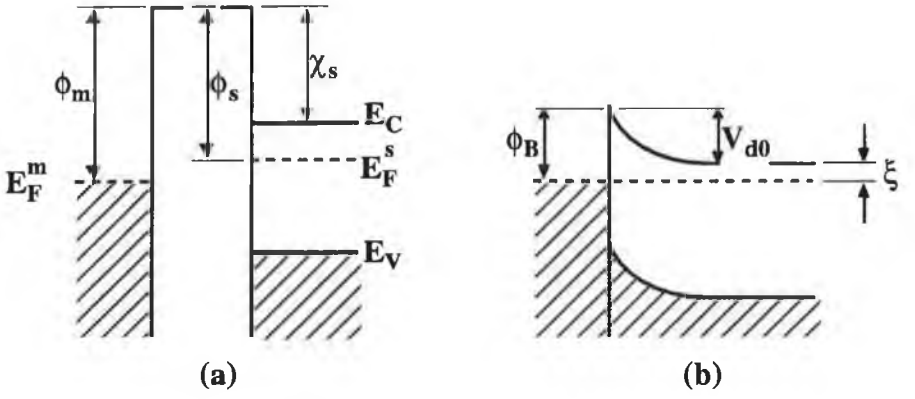

Figure 2.1 Formation of a barrier between a metal and a semiconductor.

2.2.2 I-V characterisation.

Schottky barrier diodes are majority carrier devices. Thus for an n-type Schottky barrier contact, it is mostly electrons that constitute current flow. There are four basic mechanisms in which electrons can be transported across Schottky barrier junctions under forward bias. These mechanisms are shown schematically in figure 2.2. The inverse processes occur for the case of reverse bias.

The four processes are:

1) transport of electrons from the semiconductor over the potential barrier to the metal;

2) quantum mechanical tunnelling of electrons through the barrier;

3) recombination of electrons in the depletion region;

4) hole injections from the metal to the semiconductor.

The processes 2) and 4) are only applicable for high and low doped semiconductors respectively. Diffusion of electrons through the barrier is important for low mobility semiconductors.

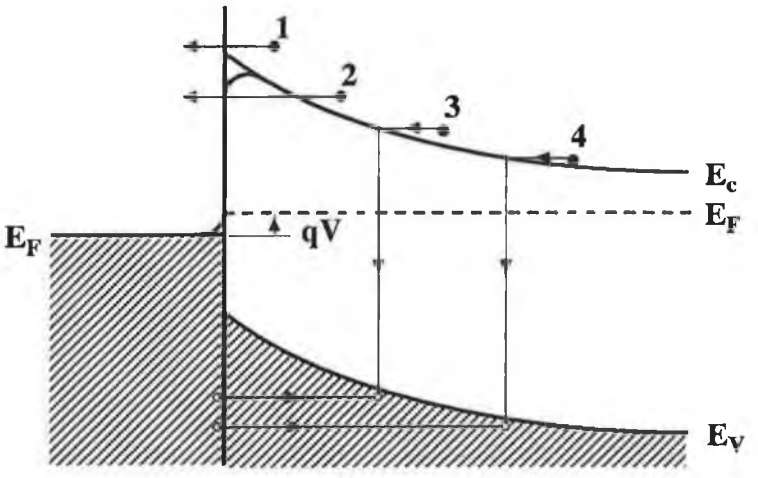

Figure 2.2 Current transport mechanisms (after [2]).

The Schottky barrier diodes in these experiments were fabricated from moderately doped (N_D-N_A = $5x10^{16}$ cm^{-3}) InP. Thus the principle mechanisms of current transport are those of recombination and thermionic emission. The current is given by:

$$I = I_s \exp\left(\frac{qV}{nkT}\right) \tag{2.1}$$

where T is the absolute temperature, I_s is the saturation current and:

$$I_s = SA^{**}T^2 \exp\left(-\frac{q\left(\phi_B^{IV} - \Delta\phi\right)}{kT}\right) \tag{2.2}$$

where S is the diode area, A^{**} is the Richardson's constant and n is the ideality factor. $\Delta\phi$ is a correlation term due to the image force lowering of the barrier. Richardson's constant takes account of the ratio of the semiconductor effective mass to the free electron mass. The ideality

factor is an important parameter, as it is effectively a measure of how well a diode obeys the thermionic emission theory. A value of n equal to 1 indicates an "ideal" diode.
If equation 2.1 is plotted for forward bias voltages, an extrapolation of the linear region of this graph to cross the y-axis gives a value for the saturation current I_s, from which the barrier height ϕ_B^{IV} can be determined, i.e.

$$\phi_B^{IV} = \ln\left(\frac{I_s}{SA^{**}T^2}\right)\frac{kT}{q} \qquad (2.3)$$

A more exact form of equation 2.1 enables the plot to extend through V=0 for reverse bias, thus permitting more accurate determination of the barrier height and ideality factor. In this case, the I-V characteristic is written as:

$$I = I_s \exp\left(\frac{qV}{nkT}\right)\left[1-\exp\left(-\frac{qV}{kT}\right)\right] \qquad (2.4)$$

This effect is shown diagrammatically in figure 2.3.

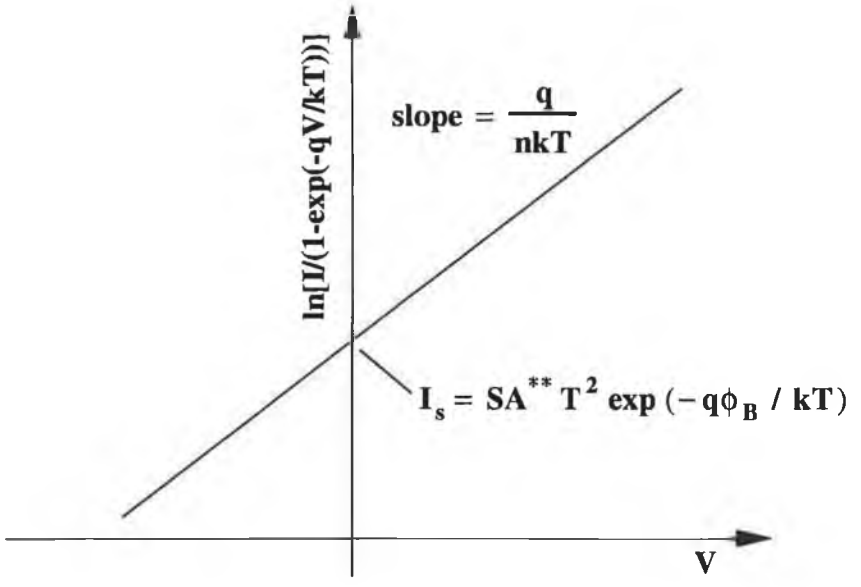

Figure 2.3 Current versus applied voltage for Schottky barrier diode.

In theory, for pure thermionic emission, the ideality factor n should be exactly 1. In practice, however, deviations from n=1 are normal and for the semiconductors used in these experiments these deviations are more pronounced in Schottky barriers under low forward bias and at low

temperatures. These deviations are mainly due to recombination of electrons in the depletion region. thus, to take account of recombination current, equation 2.4 may be rewritten as:

$$I = I_{te} - I_{rc} = \left[I_s \exp\left(\frac{qV}{nkT}\right) + I_r \exp\left(\frac{qV}{2kT}\right)\right]\left[1 - \exp\left(-\frac{qV}{kT}\right)\right] \qquad (2.5)$$

where I_{te} is the thermionic emission and I_{rc} is the current due to recombination in the depletion region as discussed earlier. Note that the assumption of a value, of n = 2, in the recombination term is a gross simplification. Nevertheless, the addition of a recombination term may be necessary for "non-ideal" diodes as failure to do so can lead to erroneous values for ϕ_B. This problem has been discussed in a paper by McLean *et al* [3].

2.2.3 C-V Measurements.

When a small ac voltage is superimposed on a reverse dc bias V_r across a Schottky diode, charges of opposite sign are induced on both the metal and semiconductor, at either side of the depletion region. As the reverse bias is increased, electrons in the conduction band recede further from the metal and increase the width of the depletion region. Similarly, if there is a significant number of holes immediately adjacent to the metal, the hole concentration will decrease because the hole quasi-Fermi level [2] coincides with the Fermi level in the metal. This change in charge gives rise to a capacitance and the diode effectively behaves as a variable capacitor. Assuming the diode is ideal and the donor concentration is uniform in the semiconductor, the differential capacitance under reverse bias is given by :

$$\frac{\partial Q_d}{\partial V} = C = S\left(qN_d\varepsilon_s / 2\right)^{1/2}\left(\phi_B^{CV} - V_n + V_r - \frac{kT}{q}\right)^{-1/2} \qquad (2.6)$$

where S is the diode area, N_d is the effective donor concentration, ε_s is the permittivity of the semiconductor. $V_n = kT/q\ln(N_0/N_d)$ is the depth of the Fermi level below the conduction band. (For the material used V_n has an approximate value of 0.06 eV). Rewriting equation 2.6 we have:

$$\frac{1}{C^2} = \left(\frac{2}{S^2 q N_d \varepsilon_s}\right)\left[\phi_B^{CV} - V_n + V_r - \frac{kT}{q}\right] \qquad (2.7)$$

Assuming ϕ_B^{CV} is independent of V_r , a plot of $1/C^2$ versus V_r should yield a straight line with an intercept V_I on the x-axis given by:

$$V_I = \phi_B^{CV} - V_n - \frac{kT}{q} \qquad (2.8a)$$

The intercept V_I is also related to the diffusion potential V_d by :

$$V_I = V_d - \frac{kT}{q} \qquad (2.8b)$$

The barrier height ϕ_B is given by:

$$\phi_B^{CV} = V_d + V_n \qquad (2.9)$$

The slope of this line gives the donor concentration.

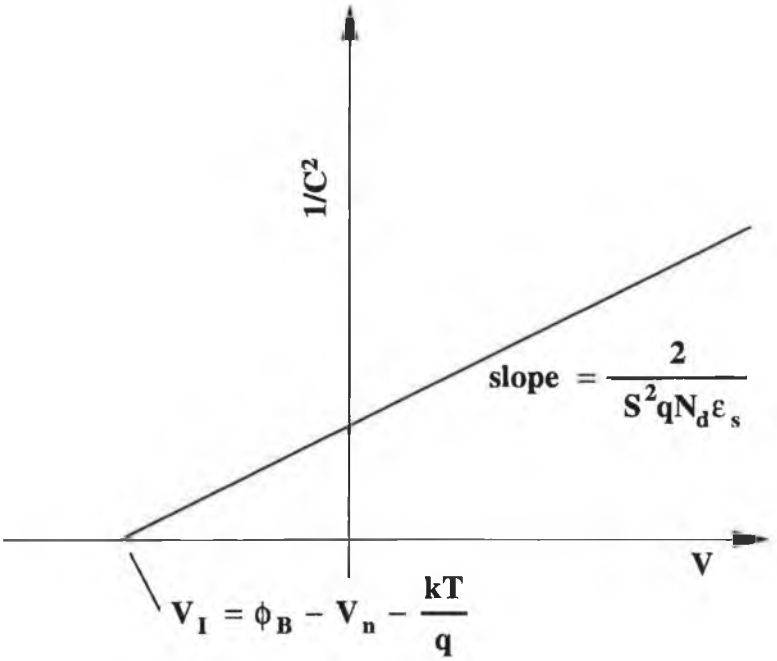

Figure 2.4 $1/C^2$ versus V plot for a Schottky barrier diode.

2.4 DLTS.

Deep level transient spectroscopy is a useful technique for defect characterisation in semiconductor devices such as Schottky barriers, p-n

junctions and metal-oxide-semiconductor capacitors. DLTS is a high frequency capacitance transient thermal scanning method for identifying a wide variety of traps in semiconductors as first discussed by P.V. Lang [4]. In addition, DLTS allows the activation energy, concentration profile and electron- and hole-capture cross sections for each trap to be measured.

The technique is described as follows:
For an n-type Schottky barrier at zero bias (figure 2.5) all electron states (conduction band, valence band and deep states) are occupied below the equilibrium Fermi level, E_F. Thus the deep level at E_T extending into the bulk is occupied below E_F and empty above E_F.

The essential features of a transient-capacitance measurement can be discussed with reference to the energy band diagrams shown in figure 2.5 (after Roberts [5] 1993) for a current rectifying metallic contact on an n-type semiconductor as was used in these experiments. The Schottky diode with barrier height ϕ_B is shown for zero applied bias in figure 2.5(a). The position of the Fermi level, E_F is shown. There is also a deep level of activation energy E_T below the conduction band extending into the bulk which is only occupied below E_F. Under zero bias conditions, the space charge layer has a depletion width W_0.
Under a reverse bias voltage V_r as illustrated in figure 2.5(b), the depletion region of $W_r > W_0$ exists in which the steady state occupation is determined by a quasi-Fermi level ξ. The reverse bias is applied to create a deep depletion space-charge layer. This is followed by a voltage pulse to induce a non steady-state occupancy of the deep levels. figure 2.5(c) shows that when a forward bias pulse $V > V_r$ is applied to the Schottky barrier diode, the quasi-Fermi level moves closer to the conduction band and the depletion region width decreases to $W < W_0$.
As an almost flat band condition exists, the deep level is now completely occupied provided the pulse duration is longer than the characteristic filling time. After the pulse the non steady-state distribution of trapped charge relaxes and electrons are emitted to the conduction band from the region of the deep level above the quasi-Fermi level. In contrast to the movement of free electrons, the electrons in the deep levels have a slow response time and are extremely temperature sensitive.

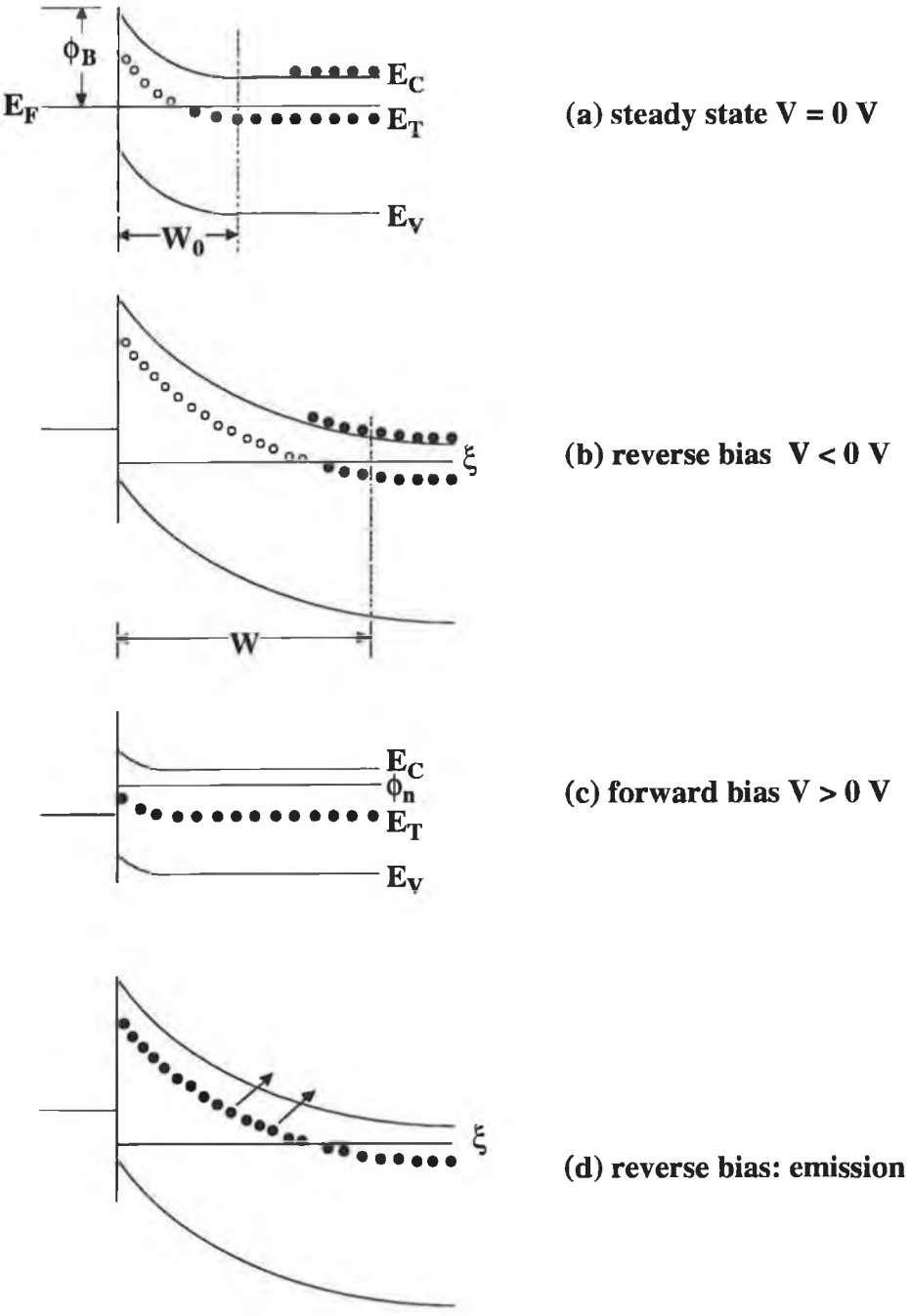

Figure 2.5 Energy band diagrams for different bias conditions. (a) zero bias (equilibrium condition). (b) reverse bias. (c) forward bias. (d) reverse bias re-established.

As the electrons are emitted to the conduction band they leave behind a (net) positive charge, causing the space charge density to increase. For a constant applied reverse bias, the increase in space-charge density causes the capacitance to increase with time. This is detected as a time varying capacitance which is measured to provide the DLTS signal.
The electron emission following the bias pulse in this situation can be

described by the following kinetic equation:

$$\frac{dn_T}{dt} = -e_n n_t \quad \left\{ \begin{array}{l} n_t = N_T \text{ at } t = 0 \\ n_t = 0 \text{ at } t = \infty \end{array} \right. \tag{2.10}$$

Where n_t is the concentration of trapped electrons and e_n is a constant known as the emission rate. Therefore:

$$n_t(t) = N_T \exp(-e_n t) \tag{2.11}$$

The trapped electron density decays with a time constant $(e_n)^{-1}$ and the positive space charge and hence capacitance builds up with the form $\approx (1 - \exp(-e_n t))$. The pulse sequence and corresponding capacitance response is illustrated in figure 2.6.

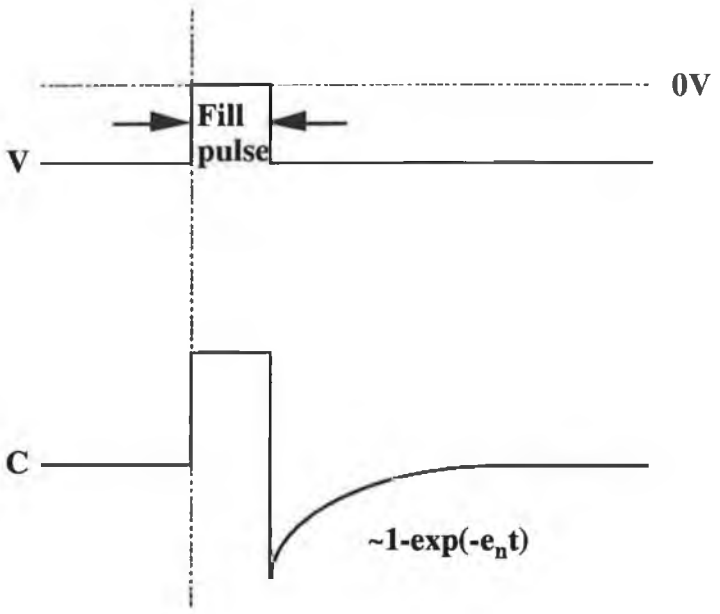

Figure 2.6 Bias pulse sequence and corresponding capacitance change (after Plaron Manual 19).

If the pulsing sequence is carried out over a range of temperatures and the capacitance transient is monitored as in figure 2.7 a DLTS signal is obtained [4]. Repetitive transient signals are fed into a boxcar averager with gates which sample at times t_1 and t_2 as shown. The signal from the differential output of the boxcar averager is the capacitance difference:

$$\Delta C = C(t_1) - C(t_2) \tag{2.12}$$

This is the DLTS signal which goes through a maximum at the temperature for which the trap emission rate equals the "emission rate window", e_0 offset by the DLTS system. The rate window depends on the delay times t_1 and t_2 as follows:

$$e_0 = (t_1 - t_2)^{-1} \ln\left(\frac{t_1}{t_2}\right) \qquad (2.13)$$

Plotting the DLTS signal over a range of temperatures gives the DLTS spectrum seen in figure 2.7.

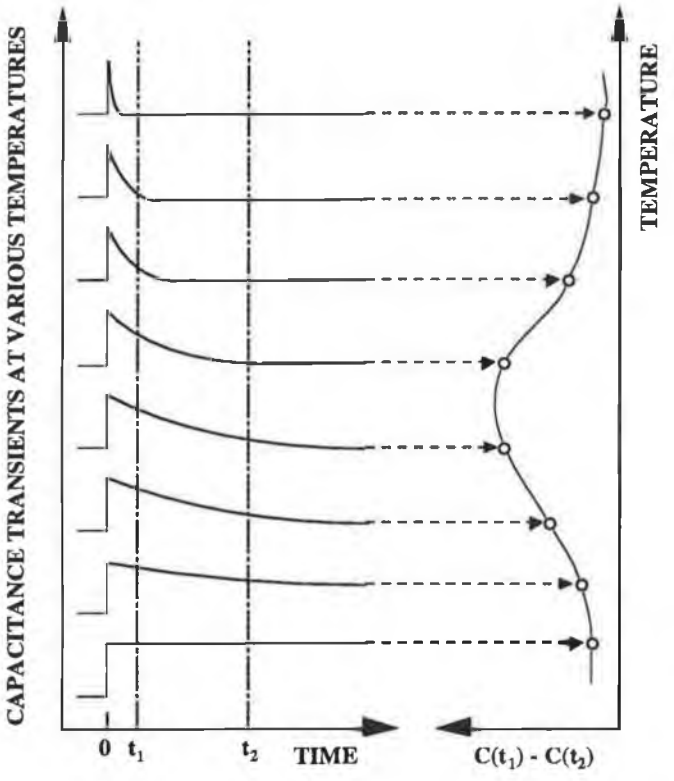

Figure 2.7 DLTS signal [4].

2.4.1 Detection of Interface States.

Interface states can be identified by DLTS techniques also despite the fact that they can have a range of energies throughout the semiconductor band gap. If a positive bias pulse is applied such that the quasi-Fermi level, ξ is moved close to the conduction band (figure 2.8 (b)) all interface states below ξ will fill with electrons. After returning to reverse bias condition (figure 2.8 (c)) electrons will be

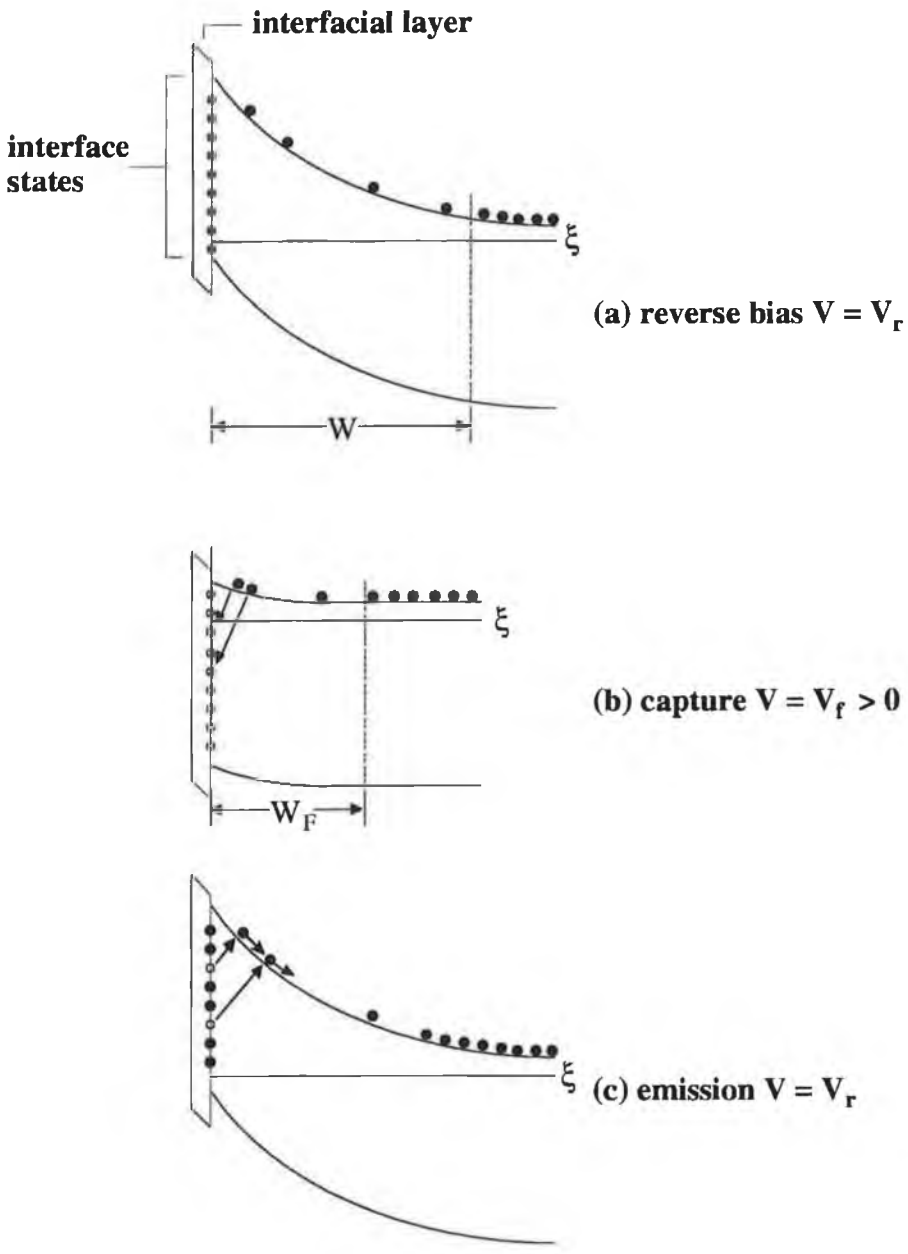

Figure 2.8 Interface state detection by forward bias DLTS: (a) Schottky barrier diode under reverse bias V_r; (b) capture process $V=V_f$; (c) emission process $V=V_r$.

emitted to the conduction band. Electrons occupying interface states situated close to the conduction band will be emitted in the shortest time. Thus if the forward bias pulse is increased in magnitude the DLTS peak associated with the interface state will be moved to lower temperature. Also, the peak intensity will increase as the interface state density is continuous up to the conduction band. It is this peak movement and increasing intensity that distinguishes broad interface state distributions from discrete bulk traps. It is possible to identify a discrete level of

interface states by forward bias DLTS as a peak whose intensity does not saturate with increasing pulse voltage provided it does not have a corresponding bulk trap at the same energy.

2.5 LEED.

Low energy electron diffraction (LEED) is a very useful surface science technique. LEED is used to determine the periodic, two dimensional arrangement of atoms at a surface. It provides a method of monitoring the arrangement of atoms at a surface and the size of the surface unit cell [6].

The basis for the interference of electrons at the crystal surface is the deBroglie [7] equation:

$$\lambda = \frac{h}{mv} \qquad (2.14)$$

This equation correlates wavelength λ with the velocity v and mass m of a flux of particles, h being Plank's constant. The wavelength for 100 eV electrons is approximately 1 Å so the interference of these waves with periodic crystal lattices is to be expected. In their paper "Diffraction of electrons by a crystal of nickel", Davisson and Gemmer [8] analysed the directions of diffraction maxima on the basis of deBroglie's equation. In 1934 Ehrenlang [9] suggested accelerating the diffracted electrons onto a fluorescent screen after passing through a system of fine grids. Lander *et al.* [10] later developed this idea to it's present day form.

Formation of a LEED pattern.

For three dimensional crystals, planes within the lattice may be defined by the Miller indices (h'k'l'). By analogy with a two dimensional structure, the lattice points may be arranged in rows classified by the indices (h'k'). The diffraction spots of a LEED pattern may be attributed to scattering at rows (h'k') and these indices can be used to describe LEED patterns. The distance $d_{h'k'}$ between neighbouring rows of direction [h'k'] is given by the equation:

$$\frac{1}{d^2_{h'k'}} = \frac{h'^2}{b_1^2 \sin^2 y} + \frac{k'^2}{b_2^2 \sin^2 y} - \frac{2h'k' \cos y}{b_1 b_2 \sin^2 y} \qquad (2.15)$$

where y is the angle between the axis of the unit cell whose base vectors

have lengths b_1 and b_2 . For a rectangular unit cell (y=90°) the equation simplifies to:

$$\frac{1}{d^2_{h'k'}} = \left(\frac{h'}{b_1}\right)^2 + \left(\frac{k'}{b_2}\right)^2 \qquad (2.16)$$

Since the interference of electrons at a crystal surface is determined by deBroglie's equation, constructive interference occurs if the scattered waves from neighbouring lattice points have a path length difference of multiples of the wavelength λ. In one dimension for a primary wave striking the surface with an incidence angle ϕ_0 , interference of the back scattered waves occurs in directions ϕ (see figure 2.9), where ϕ is given by the equation:

$$a(\sin\phi - \sin\phi_0) = n\lambda \qquad (2.17)$$

where a is the distance between the periodically arranged scatterers and n an integer denoting the order of diffraction.

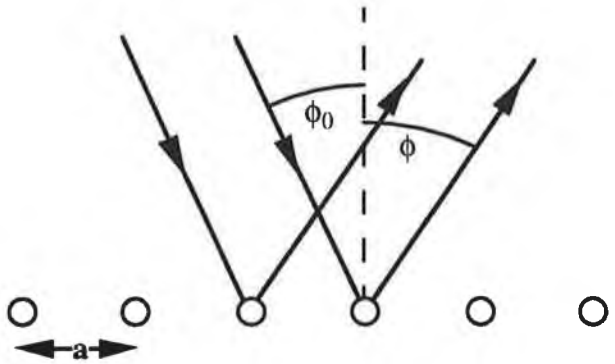

Figure 2.9 Diffraction condition.

In two dimensions an arrangement of lattice points may be considered as an ensemble of parallel rows of scatterers with directions [h',k'] and mutual distances $d_{h'k'}$. In this case interference maxima are to be expected in directions given by:

$$n\lambda = d_{h'k'}(\sin\phi - \sin\phi_0) \qquad (2.18)$$

LEED experiments are usually performed with normal incidence of the primary electrons ($\phi_0 = 0$), so that the equation simplifies to:

$$\sin\phi = \frac{n\lambda}{d_{h'k'}} \approx \frac{n}{d_{h'k'}}\sqrt{\frac{150}{U}} \qquad (2.19)$$

with the electron energy, U in eV and $d_{h'k'}$ in Å units. Each set of atomic rows, {h'k'} will therefore give rise to a series of diffraction maxima, nh',nk' with varying order of diffraction, n. The larger the unit cell, the closer the first diffraction maxima will be relative to the surface normal.

The directions can be observed directly with typical LEED apparatus and they allow the $d_{h'k'}$ to be determined and therefore the geometry of the unit cell. In order to determine the position of atoms within the unit cell it is necessary to analyse the intensities of the maxima which is a complex procedure. However, information about the size and orientation of the surface unit cell is very useful.

2.6 Auger Electron Spectroscopy.

Auger electron Spectroscopy can provide valuable chemical information about a surface. An atom which has been ionised in one of the inner (core) states may return to the electronic ground state via one of the following processes:

a) An electron in an energetically higher level fills the core hole, the energy thereby released is emitted as a quantum of characteristic X-ray radiation (figure 2.10).

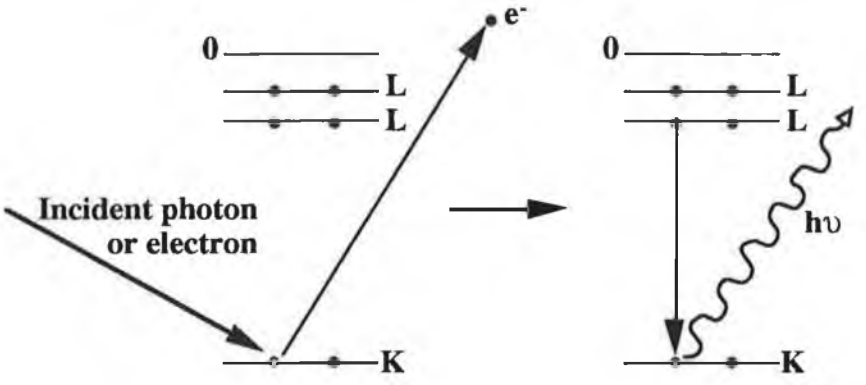

Figure 2.10 De-excitation by characteristic X-ray emission.

b) The core hole is filled by an outer electron, but the available energy is transmitted in a radiationless process to a second electron which may

then leave the atom with a characteristic kinetic energy (figure 2.11).

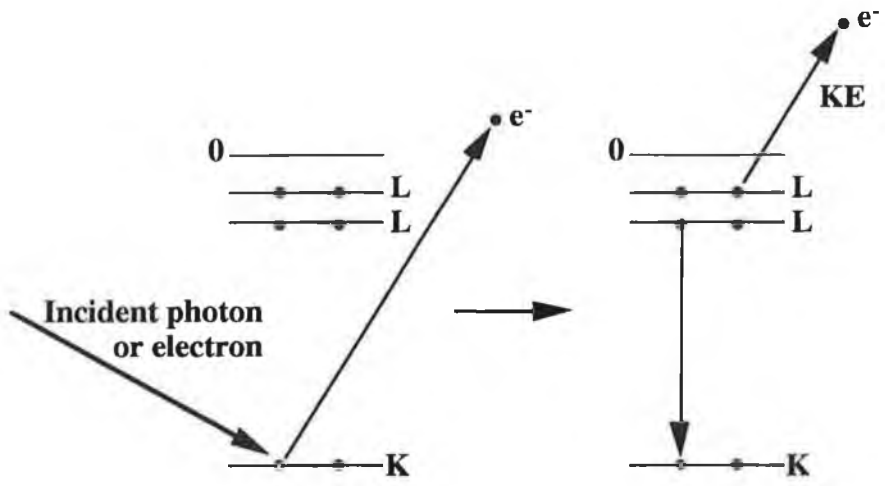

Figure 2.11 The Auger effect.

The second processes is called the Auger effect, first observed by P. Auger [11] in 1952. The kinetic energy of an Auger electron is determined by its parent atom which means that Auger is a valuable tool in elemental composition analysis. The characteristic Auger peaks are recorded for most elements and it is therefore easy to compare experimental spectra for identification purposes. The essential elements of an Auger electron spectrometer are, a source for primary excitation, an analyser and a detector system.

2.7 Introduction To Photoemission.

Photoemission is the most widely used technique for determining the electronic structure of solids. Photons absorbed by atoms in the sample result in electron transitions from filled initial states to empty final states. Some of these electrons make their way towards the surface, and those that emerge can be analysed in a detector. The mean free path of emitted electrons is a strong function of their kinetic energy (E_k) being most surface sensitive in the 40 - 90 eV range as illustrated in figure 2.12.

Angle resolved photoemission from single crystal samples allows the measurement of electron momentum as well as energy and hence an experimental determination of the electronic band structure. Angle integrated photoemission can provide information about core levels and when coupled with spectroscopic deconvolution it is suitable for the investigation of surface and interface formation because of it's

sensitivity to different chemical environments.

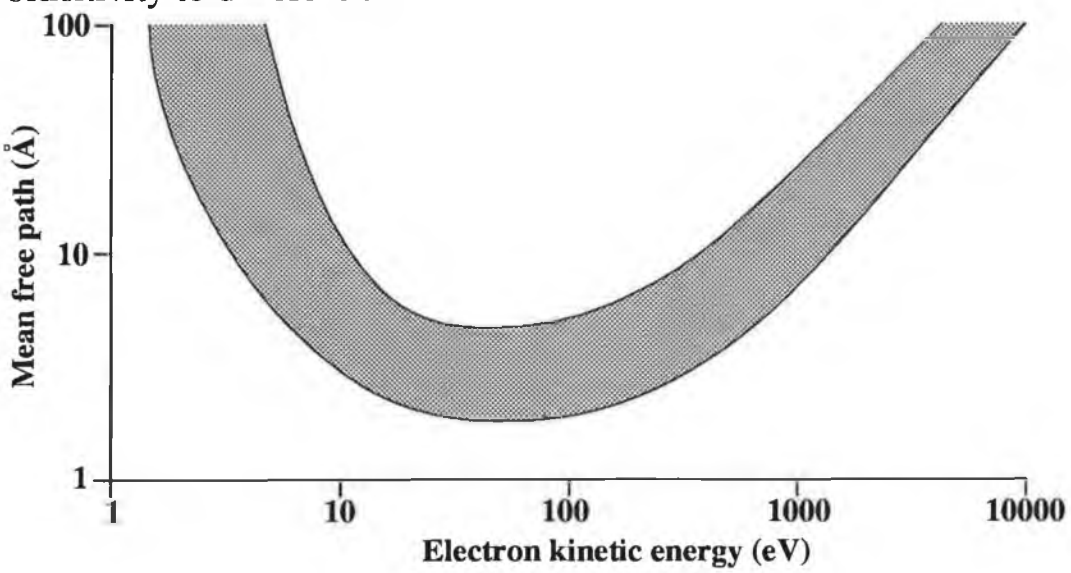

Figure 2.12 Electron mean free path versus kinetic energy.

2.7.1 The Principle of Photoemission.

Photoemission occurs when electrons are liberated from their bound state in the atom by interaction with electromagnetic radiation. The kinetic energy of these electrons (E_K) which can be measured is

$$E_K = h\upsilon + E_B \qquad (2.20)$$

where E_B is the binding energy of the electron in the atom, ϕ is the work function, h is Planck's constant and υ is the known frequency of the exciting radiation.

The simplest model used to describe this effect is the three step model proposed by Berglund and Spicer [12] which provides an approximate correlation between the measured photoelectron energy distribution and the density of electronic states in the solid. It is assumed that the optical transitions giving rise to the observed photoelectrons are the same as those which give rise to the bulk optical absorption. See figure 2.13

Step 1) Excitation of an electron into the solid from the level E_i to the level $E_f=E_i + h\upsilon$ by means of absorption of a photon with energy $h\upsilon$.

Step 2) Propagation of the excited electron into the surface of the solid.

Step 3) Ejection of the excited electron from the solid into the vacuum.

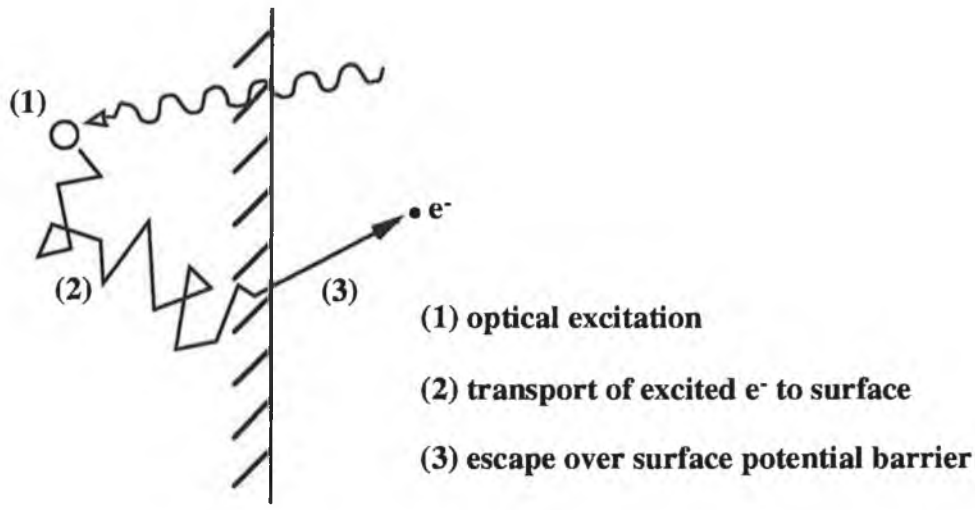

Figure 2.13 The three step model.

This model does not give a completely correct description, more complex theoretical approaches are necessary for a rigorous account, for example, the quantum mechanical one step model [13,14].

One of the fundamental problems in interpreting the photoemission spectra is that of separating the primary unscattered core level electrons from the inelastically scattered ones. In the case of the one electron band model when the reduced wave vector k is conserved it is necessary only to consider vertical transitions. This is illustrated in figure (2.14) after N.V. Smith, where an electron in a band *i* of initial states executes an optical transition to a state in a band *f* of final states. If $E_f(k)$ and $E_i(k)$ represent the energy dispersion relations in bands *f* and *i* respectively, the optical transitions at photon energy $\hbar\omega$ are confined to a surface in k-space; the equation of this surface is

$$E_f(k) - E_i(k) - h\upsilon = 0 \qquad (2.21)$$

often written as $E_K = h\upsilon + E_B - \phi$, where the kinetic energy $E_f(k)=E_K$ and $E_i(k) = E_B - \phi$.
This is known as the one electron approximation. The binding energy for core levels of common elements is well documented providing a useful reference for the experimenter. By observing intensities at various binding energies the chemical interaction of atoms at the surface of a sample may be analysed.

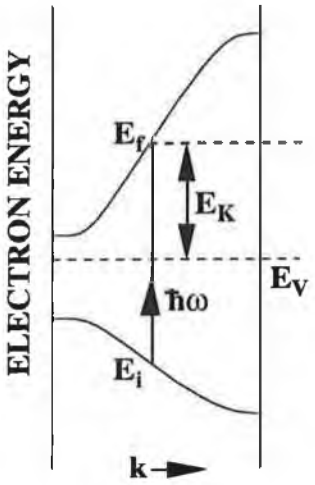

Figure 2.14 Energies of a direct transition at a point along some arbitrary direction in k-space. E_V is the vacuum level and E_K represents the kinetic energy of the photoemitted electron.

2.7.2 Angle Resolved Photoemission.

The motivation for angle resolved photoemission from solids may be stated as follows. If one has measured the kinetic energy E_K of a photoelectron and also it's direction of propagation, one has automatically measured its momentum or wave vector k. This follows from the relation

$$E_K = \frac{\hbar^2 k^2}{2m} \qquad (2.23)$$

Therefore it is possible to identify a single point in k-space rather than settle for an integrated quantity. Consider the situation in figure 2.14 where an electron has been excited into the state at $E_f(k)$, suppose this electron propagates towards the surface (step two of the three step model) and arrives without scattering. The escape across the surface is then determined by the conservation of the wave vector parallel to the surface.

$$K_{||} = k_{||} + G_{||} \qquad (2.24)$$

Here $K_{||}$ is the parallel component of the external photoelectron wave vector, $k_{||}$ is the parallel component of the reduced wave vector k, and $G_{||}$ is the parallel component of any reciprocal vector G. The photoelectron

created by the transition shown in figure [2.14] can emerge from the crystal in a number of different directions.

These directions are well defined for the following situation. If E_V denotes the energy of the vacuum level, the kinetic energy of the external photoelectron is given by

$$\begin{aligned} E_K &= \hbar^2(k_\perp^2 + k_\parallel^2)/2m \\ &= E_f(k) - E_V \end{aligned} \qquad (2.25)$$

where $K_\perp$ is the component of the photoelectron wave vector perpendicular to the surface. From (2.24) and (2.25) we have, for the (k+G) component

$$\hbar^2 k_\perp^2 / 2m = [E_F(k) - E_V] - \hbar^2(k_\parallel + G_\parallel)^2 / 2m \qquad (2.26)$$

Thus if we know $E_F(k)$ and E_V the values of $K_\perp$ and $K_\parallel$ are fixed. Therefore, given a good band structure calculation, the directions of photoelectrons generated by bulk optical transitions are completely determined [15].

Taking the argument in reverse by measuring the energies and directions of emitted photons it is possible to work backwards and deduce the E_K vs. k dispersion relations for the electronic states within the solid. Though $k_\perp$ is not defined explicitly in the above equations when angle resolved photoemission is carried out both E_K and the direction of emission can be kept constant and the photon energy $\hbar\omega$ is varied. $k_\parallel$ is then fixed and it is possible to sample the band structure as a function of $k_\perp$ along some symmetry direction.

2.7.3 Reference Level.

In order to quantify information from a photoemission spectrum it is necessary to have a reference level. In the case of a metal this is simply the Fermi level. However for a semiconductor the reference level is taken to be the valence band maximum as E_F - E_{vs}. Both a reference Fermi level and valence band maximum (VBM) will be recorded during an experiment as the VBM may shift due to band bending effects if adsorbates are chemically active with the semiconductor. When using a wide band source such as synchrotron radiation frequent Fermi level measurements on a reference metal can provide an indication of beam

energy drift.

References.

[1] W. Schottky, Naturwiss **26** (1933) p.843.

[2] E.H. Rhoderick and R.H. Williams, Metal-Semiconductor Contacts, 2nd Edition, Oxford Science Publications (1988).

[3] A.B. McLean, I.M. Dharmadasa and R.H. Williams, Semicond. Sci. Technol. **1** (1986) p.137.

[4] D.V. Lang, J. Applied Phys. **45** (1974) p.3023.

[5] L. Roberts, thesis, Dublin City University,Ireland,(1993).

[6] Ertl/Kuppers,"Low Energy Electrons And Surface Chemistry".

[7] L. de Broglie, Phill. Mag. **47** (1942) p.446.

[8] C.J. Davisson and L.H. Germer, Phys. Rev. **22** (1923) p.242.

[9] W. Ehrenberg, Phil.Mag. **18** (1934) p.878.

[10] J.J. Lander, F. Unterwald and J. Morrision, Rev. Sci. Instr. 33 (1962) p.784.

[11] P. Auger, J. Phys. Radium **6** (1925) p.205.

[12] C.N Berglund and W.E. Spicer, Phys. Rev. A **136** (1964) p.1030.

[13] W.L. Schaich and N.W. Ashcroft, Phys. Rev. B **3** (1971) p.2452.

[14] G.D. Mahan, Phys. Rev B **2** (1970) p.4334.

[15] N.V. Smith, Angular Dependent Photoemission from Solids.

Chapter 3 Passivation of InP.

3.1 Introduction.

III-V compounds are well recognised for their potential applications in high speed electronic and long wavelength optical circuitry. InP has many potential uses in optoelectronics. The band gap (1.4 eV) makes InP potentially an ideal candidate for optical devices. Due to it's high electron mobility it is useful for high speed devices and high power switching devices. InP is also ideal for microwave devices. The maximum values of the hole mobility measured in p-type InP are 150 cm^2/vs^{-1} at 300K[1] and 2200 cm^2/vs^{-1} at 77K [2]. In heavily doped samples i.e. $1x10^{18}$ cm^{-3} the maximum reported mobility is between 200-300K and reaches values between 30 and 60 cm^2/vs^{-1} [3]. The reported barrier heights for n-type Ag/InP interfaces range from 0.35 eV to 0.72 eV depending on the measurement technique and the method of substrate and interface preparation. Williams and co-workers [4,5] measured a barrier height of 0.5 eV at the cleaved Ag/InP interface using a combination of photoemission, IV and CV techniques . However there is a large obstacle to this realisation, due to the fact that InP has a high density of surface states. This results in the Schottky barrier height being low and unpredictable. The behaviour of diodes fabricated on untreated InP surfaces is erratic and by looking at the diagram below (figure 3.1), one can see the effect of the interface states. The interface states provide an alternative route for electrons reducing the rectifying properties of the Schottky diode.

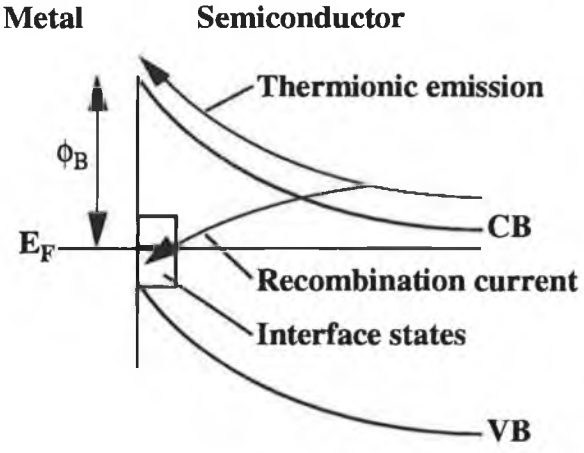

Figure 3.1 Interface states at metal-semiconductor interface.

For unpassivated InP, the recombination current tends to be very high, thereby greatly affecting the diode performance. Thus, there is a great interest in any methods that can passivate InP or reduce this recombination current. There have been a wide range of studies on this matter including dry etch techniques, wet chemical etch techniques, oxidation and the laying down of an insulating layer between the semiconductor and the metal over layer. Gold, silver, aluminium and many other metals have been tried with the aim of reducing the density of interface states and improving device ideality. As part of this work a wide variety of these techniques were tried and tested. The most revealing was wet chemical etching of InP with ammonium polysulphide followed by a rapid anneal at high temperature.
Compared to the enormous amount of literature devoted to deep level transient spectroscopy on GaAs, the corresponding data for InP is rather limited. This is partly due to the fact that there are no recognised systematic deep levels associated with the growth techniques of InP. Usually for InP the concentration of deep levels detected is only in the range 10^{14} - 10^{15} traps /cm^3, compared to commonly 10^{15}-10^{16} traps/cm^3 in GaAs [6]. Also as mentioned the barrier height is rather small on InP.

3.2 Review.

Interest is increasing in InP based devices as microwave field effect transistors (FETs) metal-insulating-semiconductor field effect transistors (MISFETs) and as compounds for optical fibre communications. This is mainly due to their high saturation drift velocity, high mobility and low ionisation coefficients. There are two major problems with InP, it has a high interface state density causing current drift and it is thermally unstable, thermal degradation has been reported at temperatures as low as 200°C[11].
In 1984 A. Guivarch *et al.* [7] reported results from n-type InP(100) which had been accidentally cleaned using 12 different etching procedures. They highlighted an NH_4OH etch as the one which produced the most ideal results. Forest and Schmidt [8,9] published two papers in 1984 and 1986 discussing the improvement to InP diode performance that could be achieved by making organic and inorganic semiconductor contact barrier diodes using PTCDA, which is an organic insulator which can be molecularly evaporated. They reported to have improved diodes due to enhanced contact barriers and reduced edge effects.
Chave [10] investigated arsenic passivation of InP surfaces using an

As-based aqueous chemical treatment and a molecular-beam epitaxy technique. He found that both the techniques resulted in improved electronic and physiochemical properties of the InP surface. He reported a reduction in the density of surface states, suppressed drift and enhanced thermal stability (similar to a follow up study on phosphorous treatments).

In 1988 Iyre, Chang and Lile [11] compared the effect of phosphorous and sulphur on the surface properties of InP in insulating gate devices. While they found the phosphorous to considerably improve the interface of InP MIS structures they reported that sulphurised InP MIS structures treated in $(NH_4)_2S_x$ exhibited excellent interface quality when high frequency and quasi static CV measurements were carried out. In a follow up study [12] they found a near ideal passivated InP surface could be achieved using liquid and gas phase sulphur treatments. The liquid preparation involved immersing the InP in a stirred and heated solution of $(NH_4)_2S_x$ while the gas phase preparation was carried out in a CVD reactor. Following either preparation a SiO_2 layer of ~600Å was grown on the passivated surface. CV measurements showed the technique to form MIS structures with low interface state densities and stable electron performance. They also reported the process as 'very repeatable'.

Oxidation has long been considered as a means of passivating surfaces and UV/ozone treatments have gained interest due to numerous applications in semiconductor surface cleaning and passivation. Hollinger *et al* [13] using x-ray photoelectron spectroscopy (XPS) discussed the ability of non-stoichiometric InP native oxides to passivate InP surfaces and they found that the oxides were stable between 30-500°C. They concluded that non-stoichiometric oxides can have beneficial electrical and passivating properties, provided that each atom has reached its maximum valency (zero defects).

Yamada, Spicer *et al* [14] also investigated thermal stability of barriers at Au and Ag/InP interfaces with Sb interlayers using photoemission. They concluded that the barriers were stable up to 200°C but suggested that optimisation of the passivation condition might improve thermal stability.

In 1991 Hurahro, Oigawa *et al* [15] compared the effect of $(NH_4)_2S_x$ treatments on the surface of III-V semiconductors by means of Auger electron spectroscopy (AES) and reflection high energy electron diffraction (RHEED). It was concluded that sulphur atoms bonded to the semiconductor surface preventing surface adsorption thereby leading to

a reduction in the surface state density. The also reported that the structure and effect of the $(NH_4)_2S_x$ treatment on the surfaces of all III-V compounds was qualitatively the same.

Tao *et al.* [16] achieved a highly stable crystalline S-passivated InP (100) surface using an illuminated and heated wet chemical $(NH_4)_2S$ solution. A (1x1) LEED was observed for up to three days after passivation and photoemission studies revealed that a monolayer of sulphur terminated the surface forming bridge bonds only to indium surface atoms. After carrying out a variety of surface preparation treatments Ingrey [17] reported on the disparity in defining clean surfaces and suggested standard procedures for defining surfaces.

Nakamuna *et al.* [18] investigated the effect of UV oxidation on barrier height of InP diodes using I-V and C-V techniques. While they found that UV-oxidation improved barrier height they found a discrepancy among the different barrier height calculations. Yhey [14] suggested that it was due to electron tunnelling through the UV oxide layer. An scanning tunnelling microscope (STM) study of sulphur treated InP by Kurihara *et al.* [19] showed a major reduction in surface roughness.

3.3 Experiment.

In these experiments polished silicon doped n-type InP with a carrier concentration of 10^{16} cm^{-3} was used. Samples were etched using the following procedure. Initially each InP sample was degreased in acetone then in methanol. The samples were then immersed in H_2SO_4 for one minute. Following this they were etched in H_2SO_4:H_2O_2:H_2O the ratio 5:1:1 for three minutes, then plunged into a P_2S_5:$(NH_4)_2$:S_x mixture (20mg P_2S_5 added to 20 ml of $(NH_4)_2S_x$ stirred and left for 5 minutes then added 60 ml of H_2O) held at 55°C for 10 minutes. Finally each sample was rinsed in high grade methanol and blown dry in an N_2 atmosphere. Unpassivated samples were prepared in the same manner but without the 10 minutes in the P_2S_5:$(NH_4)_2$:S_x mixture.

An ohmic contact of InGa paint was then applied to the non polished side of the sample and the samples were annealed at temperatures of between 350°C and 500°C in a N_2 atmosphere for one minute. Further sets of samples were prepared as before, some with the sulphur treatment and some just etched with H_2SO_4:H_2O_2:H_2O following the degrease procedure. These samples were annealed to 850°C for 30 seconds. The samples were immediately transferred to a UHV vacuum system where diodes of area 0.6 mm^2 were fabricated by evaporating Au or Ag on a hot filament as shown in figure 3.2.

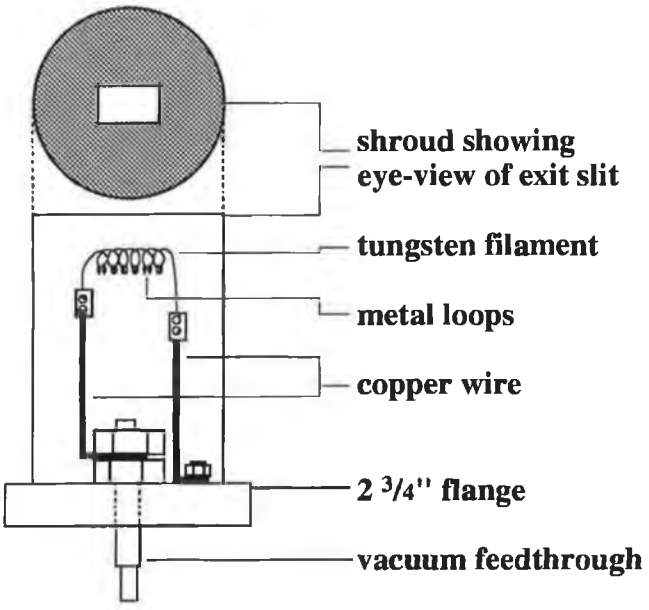

Figure 3.2 Hot filament evaporation.

These samples were then mounted on an insulating layer of mica using a conducting paint (colloidal silver) which was dried using a hot air gun. The mounted samples were placed in the cryostat sample holder illustrated below (figure 3.3) and IV and CV measurements taken for a large number of diodes on each sample. The IV measurements were taken by biasing the sample and measuring the current flowing across the device using a Keithley picoammeter. The process which was fully automated is illustrated schematically in figure 3.4. Ideality and barrier height were calculated as discussed in chapter 2.

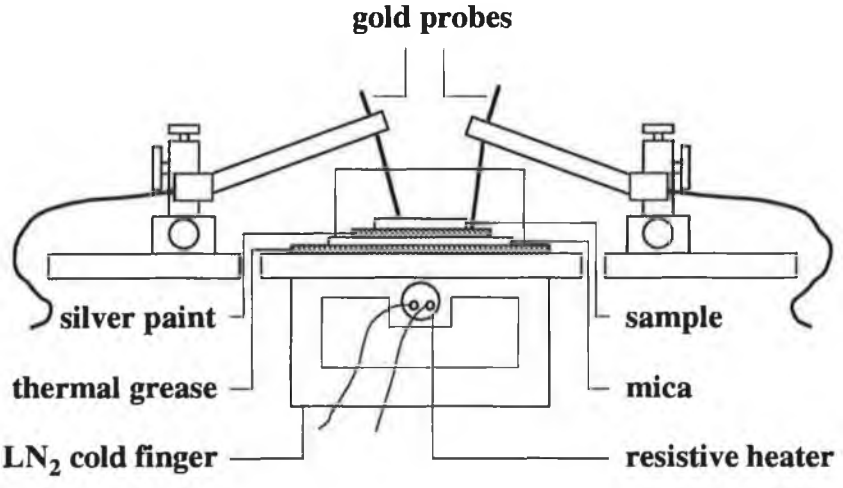

Figure 3.3 Cryostat and sample mounting arrangement.

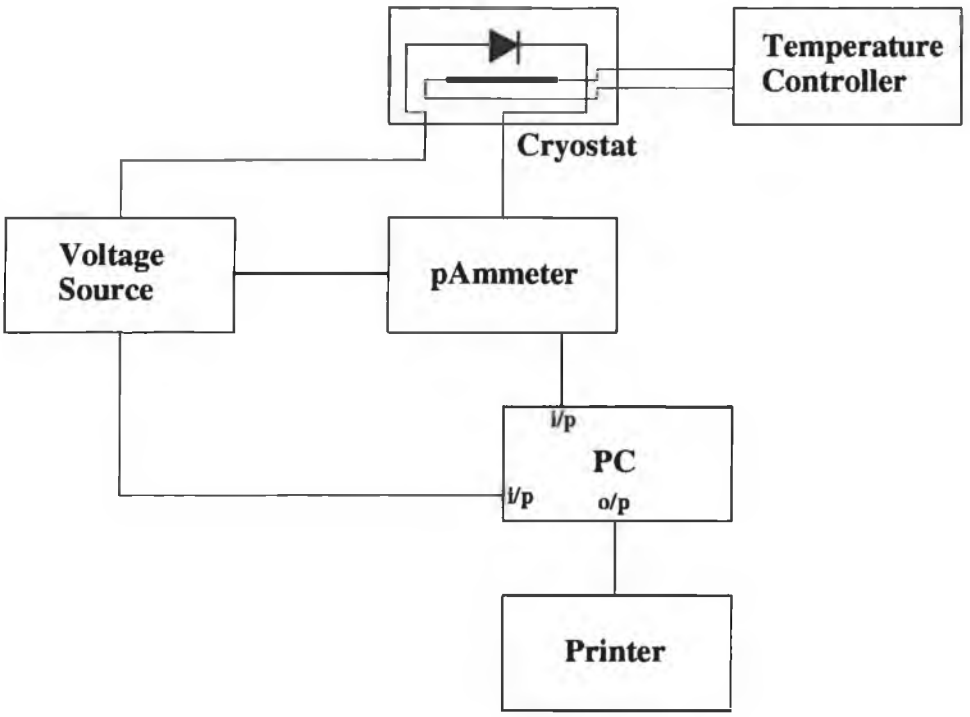

Figure 3.4 Block diagram of Current-Voltage measurement.

For the CV measurements a Boonton capacitance meter was used (see figure 3.5). This process was also automated and the software calculated the barrier height and the doping density of each sample.

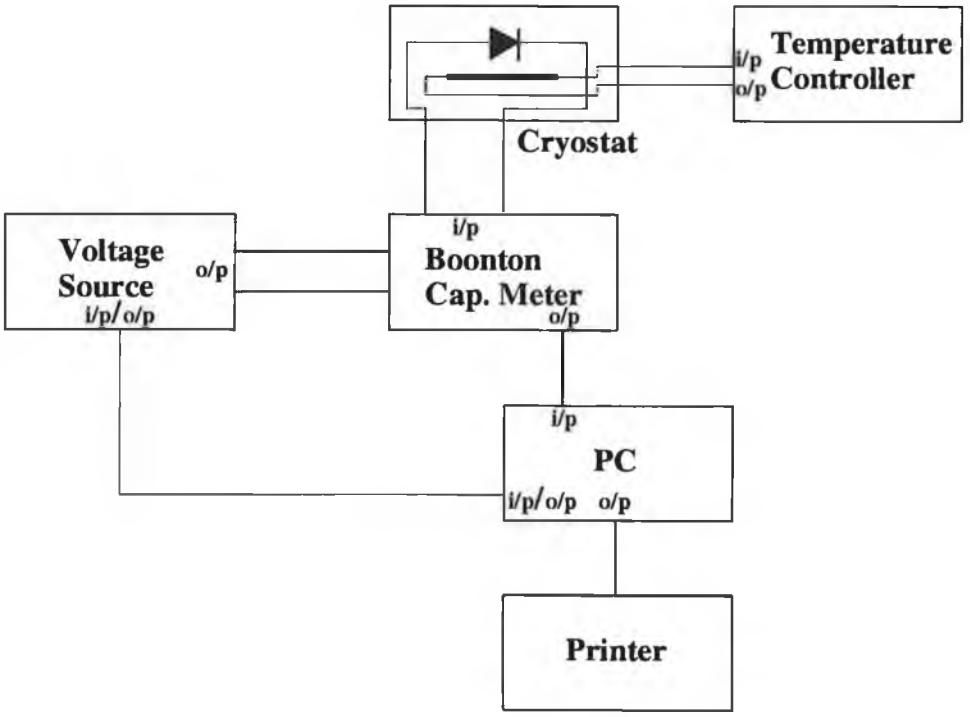

Figure 3.5 Capacitance-Voltage measurement.

In order to detect the presence of deep levels and interface states and also to calculate the activation of any deep levels and their cross section Deep level Transient Spectroscopy measurements were made. The Polaron 54600 modular DLTS system and Boonton capacitor were used (see figure 3.6). DLTS spectra were recorded over a wide temperature range from 100K to 400K and for a variety of rate windows.

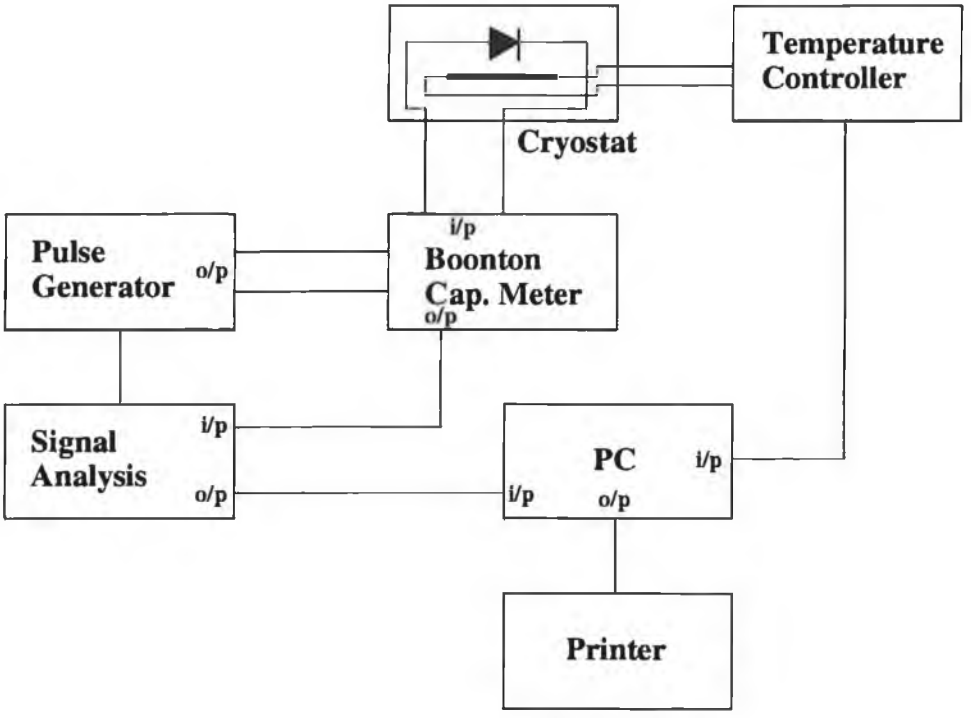

Figure 3.6 Apparatus for Deep Level Transient Spectroscopy.

3.4 Results.

From the analysis of fabricated diodes it was found that unpassivated samples had a range of idealities and their reverse currents were large, typically 50 mA, and varied even over the surface of a single diode. They exhibited a range of low barrier heights up to 0.5 eV and rectified only over a small voltage range. They exhibited no deep level traps. It was impossible to quantify the interface states as the leakage current was so large that DLTS measurements were impossible above 300K.

Sulphur treated InP showed a marked improvement in reproducibility. The reverse leakage currents were reduced greatly to typically 4.2 mA. The was some variation due to the variable nature of chemical etching but the barrier height became generally reproducible across samples and was increased to 0.6 eV. The reduced leakage currents made DLTS possible over a wider temperature range up to 350K. No interface states

or bulk traps were observed. The diodes' ideality was now fairly constant at 1.2, see table 3.1.

Sample Type	Ideality	I(reverse) (μA)	ϕ_B (eV)
Unpassivated	1.08	50	varied
Passivated	1.20	4.2	0.60
Passivated & annealed (648K)	1.13	0.74	0.49
Passivated & annealed (823K)	1.54	0.006	0.74
Passivated & annealed (873K)	1.69	0.008	0.60

Table 3.1 Idealities, reverse current and barrier heights for InP samples.

InP samples that had been sulphur treated and then annealed to 820K were also tested. Diode ideality displayed a degradation though the reverse current was reduced to nA's and ϕ_B increased to 0.7 eV. The reduction of ideality which can be observed in figure 3.7 was accompanied by the introduction of deep levels into the bulk with an activation energy of 0.678 ± 0.02 eV and interface states observed using DLTS (see figure 3.8). This results imply that the sulphur has migrated into the first few layers of the InP changing its electronic properties.

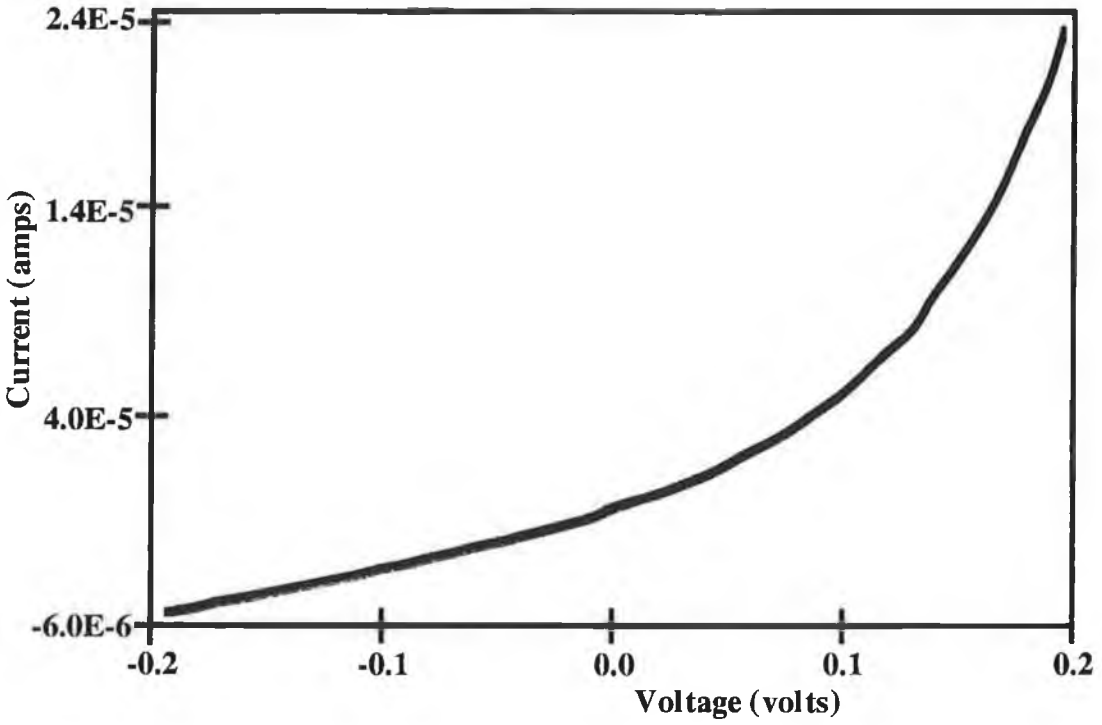

Figure 3.7 IV characteristics of S-annealed InP.

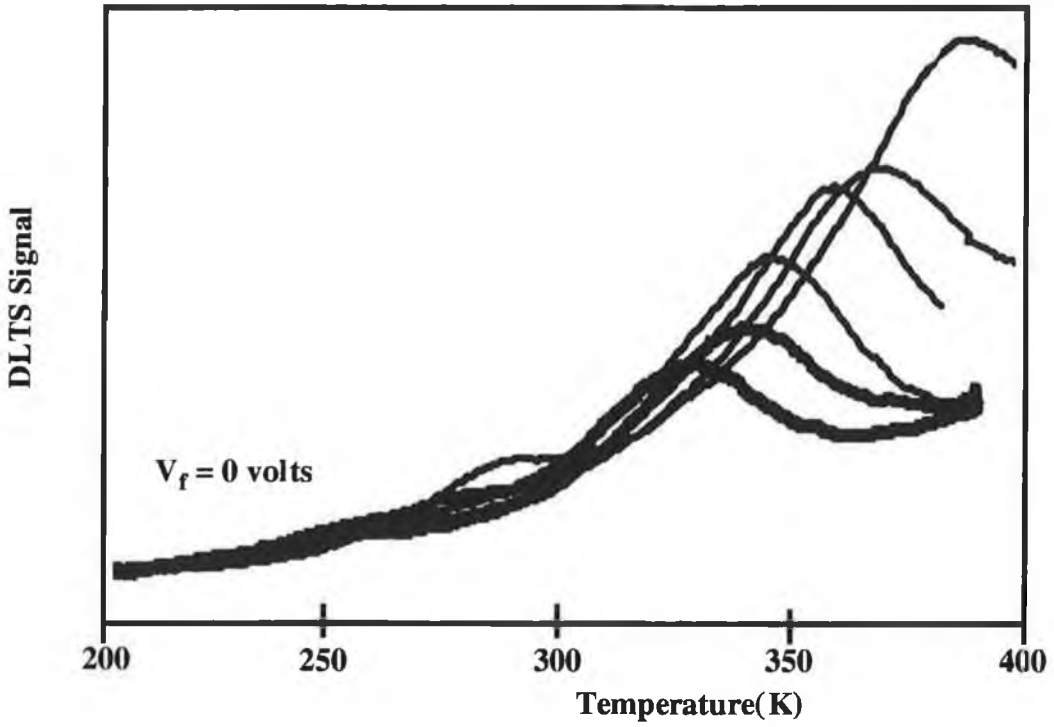

Figure 3.8 DLTS spectrum of S-annealed InP.

3.5 Discussion.

From the results obtained it is possible to come to the following conclusions. Diodes fabricated on chemically etched InP samples which have not been sulphur treated exhibit unpredictable electrical behaviour due to the large number of surface states that exist. This results in a large recombination current which hampers the device performance by reducing the barrier height and the voltage range over which the device rectifies. The InP samples that were analysed in this experiment exhibited no deep levels in DLTS and their recombination current was too large to allow the density of surface states to be measured.

The improvement in device performance of sulphur treated samples can be explained by the sulphur having a passivating effect on InP. The sulphur treated diodes rectified over a larger voltage range than the untreated samples. They had a significantly lower leakage current allowing a meaningful DLTS study of the interface states to be achieved which indicated that there were no deep levels or interface states present. This finding is in agreement with the improvement in device ideality.

From the study of high temperature annealed passivated samples, it appears that the sulphur is migrating into the InP and acting as a dopant and thus changing the electrical properties of the InP diodes. This is observed in the appearance of well defined deep levels and interface states. There is further evidence that the electronic structure of the InP has been altered by the degradation in diode ideality.

On the completion of this study it was decided the wet chemical approach to passivation was limited in it's applications as it was difficult to reproduce conditions exactly. It was decided to use instead a vacuum compatible method of sulphur deposition for further studies. This is discussed in the following chapters.

References.

[1] M. Glicksman, K Weiser, J. Phys. Chem. Solids (UK) **10**(1959) p.337-340.

[2] W. Siegel, G. Kuhnel, H. Koi, W. Gerlach, Phys. Satus Solidi A (East Germany) **95**(1) (1986) p.309-316.

[3] V.V. Galvanou, S. G. Metrevel, N. V. Siukaev, S. P. Starosel'tseva, Sov. Phys. Semicond. (USA) **13** (1969) p.94.

[4] R. H. Williams, R.R. Varma, A. McKinnley J. Phys. C (UK) **10**(22) (1977) p.4545-57.

[5] A. Mckinnley, A.W. Parke, R.H.Williams J. Phys. C(UK) **13**(36) (1980) p. 6723-36.

[6] A. Sibille, Properties of Indium Phosphite, Inspec (1990) p.239.

[7] A. Guivarc'h et al. J. Appl. Phys. **55**(4) (1984) p.1139-48.

[8] S.R. Forrest, M.L. Kaplan and P.H. Schmidt, J. Appl. Phys. **55**(6) (1984) p.1492-98.

[9] S.R. Forrest and P.H. Sghmidt, J. Appl. Phys. **59**(2) (1986) p.513.

[10] J. Chave et al., J. Appl. Phys. **61**(1) (1987) p.257-60.

[11] R. Iyer, R.R. Chang and D.L. Lile, Appl. Phys. Lett **53**(2) (1988) p. 134-36.

[12] R. Iyer, R.R. Chang, A. Dubey and D.L. Lile, J. Vac, Sci. Technol. B **6**(4) (1988) p.1174-79.

[13] G. Hollinger, D Gallet and M. Gendry, Appl. Phys. Lett. **59**(13) (1991) p.1617-19.

[14] M Yamada, A.M. Green A. Herrera-Gomez, T. Kendelewicx and W.E. Spicer, Appl Phys. Lett, **59**(24) (1991) p.3121-23.

[15] H. Oigawa, J. Fan, Y. Nannichi, H. Sugahara and M. Oshima, Jpn. J. Appl. Phys. **30**(3a) (1991) p.L322-25.

[16] Y. Tao, A. Yelon, E. Sacher, Z.H. Lu and M.J. Graham, Appl. Phys. Lett. **60**(21)(1992) p.2669-71.

[17] S. Ingrey, J. Vac. Sci. Technol. A **10**(4) (1992) p.829-36.

[18] Nakamura, et al. Jpn. J. Appl. Phys. **32** (1993) p. 699-703.

[19] K. Kurihara, Y. Miyamoto and K. Furuya, Jpn. J. Appl. Phys. **32** (1993) p.L444-46.

Chapter 4 Electronic structure of GaAs(111)B and S-GaAs(111)B.

4.1 Introduction.

In order to carry out an electronic characterisation of the GaAs(111)B clean and sulphur treated surface an angle resolved photoemission study was carried out on station 6.2 at Daresbury Synchrotron Radiation Source in the UK. Using angle resolved ultra-violet photoelectron spectroscopy (ARUPS) it is possible to band map the clean and passivated GaAs surfaces. This provides detailed information on the electronic structure of the surface and can indicate evidence of electronic surface passivation.

Though the GaAs(100) surface is currently the technologically important surface, the GaAs(111)B surface shows promise in the optoelectronic industry. A number of novel devices would be possible if it were possible to control the Fermi level pinning by electronically passivating the GaAs surface. As discussed in chapter 2, the Schottky barrier height is determined by the equilibrium position of the Fermi level in the band gap and determines the characteristics of the rectifying junction.

In this study the GaAs(111)B (2x2) reconstructed clean surface (see figure 4.1 for surface geometry) was band mapped along the major symmetry directions, as was the (1x1) S-GaAs(111)B surface. The electronic structure of clean GaAs(111)B has been investigated before using ARUPS [1] but previously the surface was prepared by Ar^+ bombardment and annealing which gives a defect rich surface. For this experiment As capped GaAs samples [2] were used, therefore it was possible to get a clean reconstructed (2x2) surface by heating the sample to 350°C so that the arsenic cap was desorbed.

4.2 Review.

Numerous investigations during the last decades have been devoted to studies of the surface electronic structure of compound semiconductors. Yet even for GaAs(110), which is the best characterised surface [3,4] the only point upon which general agreement is reached is the absence of surface states within the fundamental band gap [5].

The most comprehensive study of the GaAs(111)B surface so far was by Brigans and Bachrachn in 1984 [1]. This study experimentally identified surface states near the top of the valence band and illustrated that the

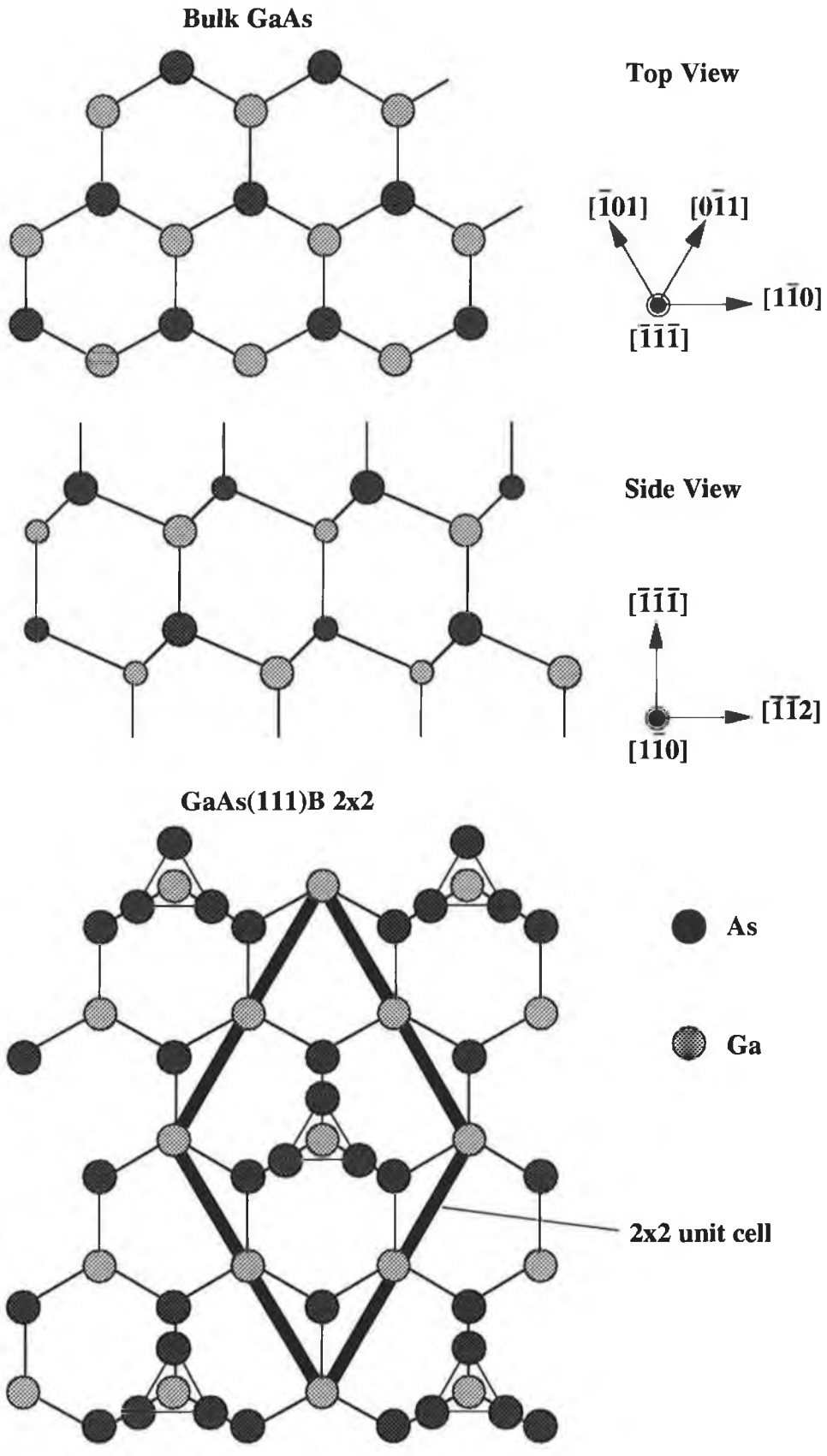

Figure 4.1 GaAs bulk and GaAs(111)B surface geometry.

local geometries of the unit cells for GaAs(111)A and (111)B were

distinctly different for a (2x2) reconstruction. Though many core level studies have been carried out on the (111)B surface ARUPS on this surface has largely been ignored.

4.3 Theory behind the Experiment.

ARUPS is a very powerful technique. In order to obtain information about the band structure one must first choose the symmetry directions of the sample along which one intends to map. This means working in k-space. Below figure 4.2 illustrates the projection of the bulk Brillouin zone on to the surface Brillouin zone for the (111) surface of a face centred cubic crystal.

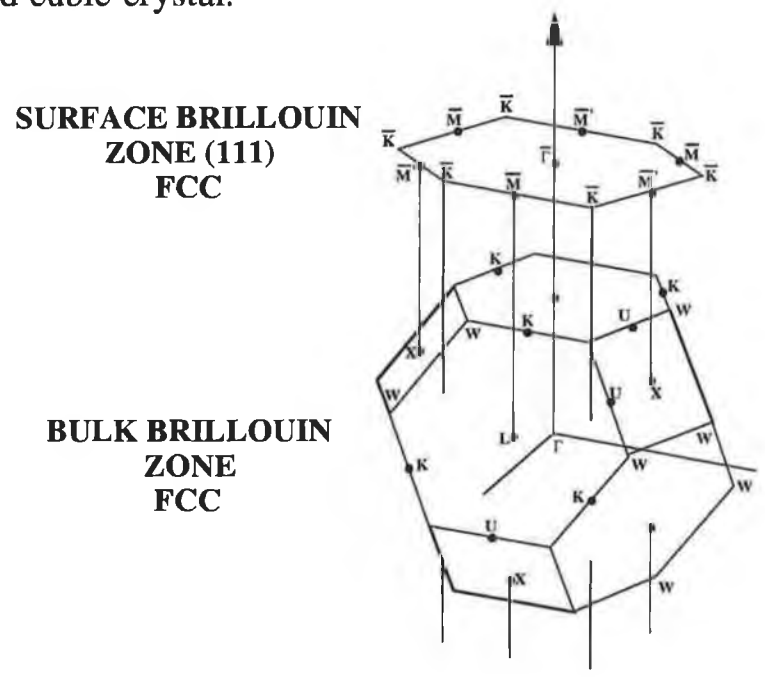

Figure 4.2 Projection of the bulk Brillouin zone onto the surface Brillouin zone for the (111) surface of a face centred cubic crystal.

Consider first the GaAs(111)B surface geometry. The GaAs(111)B (2x2) reconstructed surface will have the surface Brillouin zone illustrated in figure 4.3. The surface unit cell vector can be expressed as

$$\bar{r} = m\bar{a} + n\bar{b} \qquad -\infty \leq m, n \leq \infty \qquad (4.1)$$

for an emitted electron in k space

$$E_f(k) - E_i(k) - \hbar\omega = 0 \qquad (4.2)$$

where E_i is the electrons initial state, E_f is it's final state and $\hbar$ is

Planck's constant/2π. The kinetic energy of the ejected electron is given by

$$E_K = \hbar\omega + E_B - \phi \tag{4.3}$$

where E_B is the binding energy, and ϕ is the work function of the analyser. Since

$$E_K = \frac{\hbar^2 k^2}{2m} \tag{4.4}$$

we can say

$$k_{\parallel} = \sqrt{\frac{\hbar^2}{2m}}\sqrt{E_K}\sin\theta = 0.51\sqrt{E_K}\sin\theta \quad \text{Å}^{-1} \tag{4.5}$$

$$k_{\perp} = \sqrt{\frac{\hbar^2}{2m}}\sqrt{E_K}\cos\theta = 0.51\sqrt{E_K}\cos\theta \quad \text{Å}^{-1} \tag{4.6}$$

for the (111) face of a face centred cube [3]

$$\overline{\Gamma K} = \frac{\sqrt{2}\pi}{a\cos^2 30^\circ} \tag{4.7}$$

$$\overline{\Gamma M} = \frac{\sqrt{2}\pi}{a\cos 30^\circ} \tag{4.8}$$

where a is the lattice constant and $\overline{\Gamma M}$ and $\overline{\Gamma K}$ are symmetry directions shown in figure 4.2.

For GaAs the lattice constant a = 5.65321 Å, therefore

$\overline{\Gamma M}$ = 0.908 Å^{-1}
$\overline{\Gamma K}$ = 1.048 Å^{-1}

using Pythagoras's theorem

$$\left(\overline{\Gamma K}\right)^2 + \left(\overline{KM}\right)^2 = \left(\overline{\Gamma M}\right)^2 \tag{4.9}$$

$$\therefore \ (\overline{\Gamma M}) = 0.5232 \ \text{Å}^{-1}$$

$$\text{so} \ (\overline{\Gamma KM}) = 1.5713 \ \text{Å}^{-1}$$

Thus we have calculated the distance between the major symmetry points of the surface Brillioun zone. By using LEED it is possible to align the sample such that when the analyser is rotated it detects electrons emitted from points along the major symmetry directions.

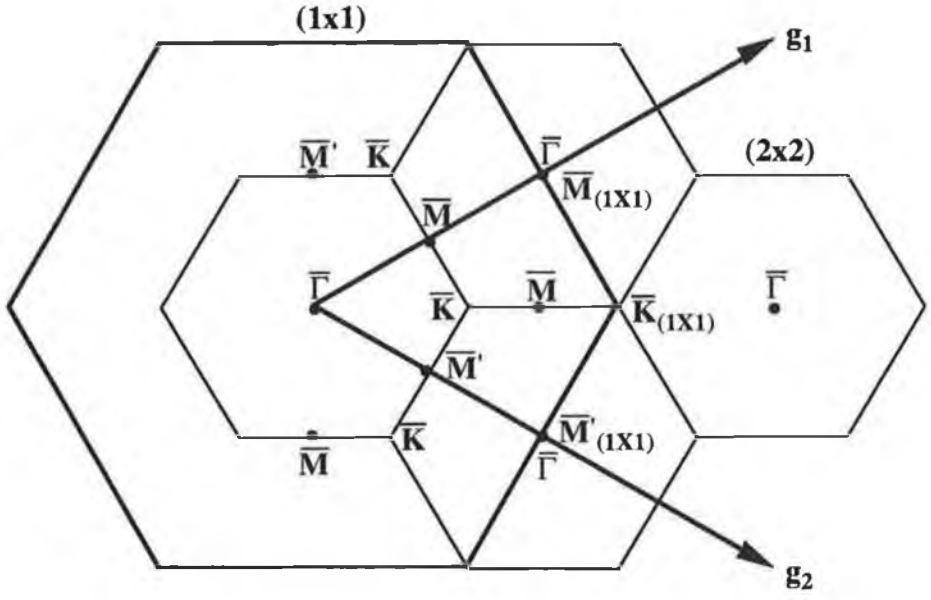

Figure 4.3 Principle symmetry directions in surface Brillouin zone.

4.4 Experimental.

4.4.1 The Beam Line.

The experiment was carried out on station 6.2 at Daresbury SRS. The synchrotron radiation arrives at the chamber via two pre focusing mirrors, a diffraction grating and two post focusing mirrors.

The white light from the SRS is deflected and focused on the entrance slit of the toroidal grating monochromator by the two prefosusing platinum coated SiC premirrors. The light is monochromated by the toroidal, gold coated, laminar, fused silica grating of either 710 1/mm or 1800 1/mm line density grating. Grating 1 covers the energy range 15-45 eV and grating 2 covers 40-110 eV. The grating focuses the monochromated light at the exit slit. The size of the exit slit determines the energy resolution of the monochromated light at the lower range of energies of each grating. At the upper range of energies of each grating

other effects such as aberrations dominate the resolution. The light is then focused on to the sample position by an ellipsoidal, gold coated post focusing mirror. This provides a final spot size of 1 mm x 2 mm at the centre of the chamber and a photon flux of $>10^{11}$ photons/second in a 0.3% bandpass (at 2 GeV 100 mA). In order to make the beam incident on the sample in the horizontal plane a plane gold coated mirror is placed before the ellipsoid mirror.

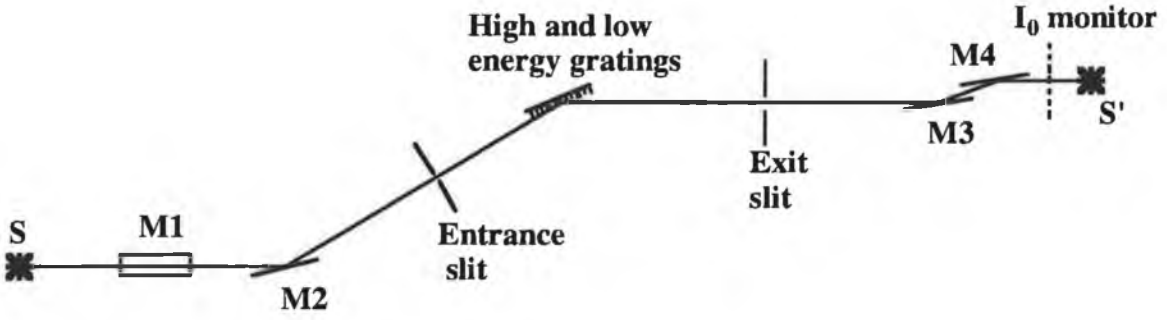

Figure 4.4 Plan of layout of TGM on beam line 6 after [7].

The main experimental chamber is a non-magnetic μ metal chamber pumped by a turbomolecular pump and two titanium sublimation pumps. The base pressure in the chamber after bakeout was $1x10^{-10}$ mbar. The samples were introduced to the main chamber by a linear transfer mechanism via a fast entry load lock.

4.4.2 Sample Preparation and Manipulation.

The samples used were MBE grown GaAs epi-layers doped with silicon atoms to $1x10^{18}$ cm^{-3} and subsequently capped in situ with a protective arsenic layer [2]. The GaAs samples were cleaved from wafers to approximately 10 mm x 5 mm. Each sample was mounted on a molybdenum sample spade with molten indium by heating the spade to 145°C on a hot plate and placing the sample on the molten indium. The spade was then allowed to cool and the sample remained adhered to the sample spade.

The spade and sample were then mounted on a carousel type holder in the introduction lock. Sample transfer to the main chamber was achieved via a gate valve. A wobble stick was used to withdraw the sample spade from the carousel and slide it into the holder at the end of the manipulator. The linear translator was then withdrawn from the main chamber and the gate valve closed.

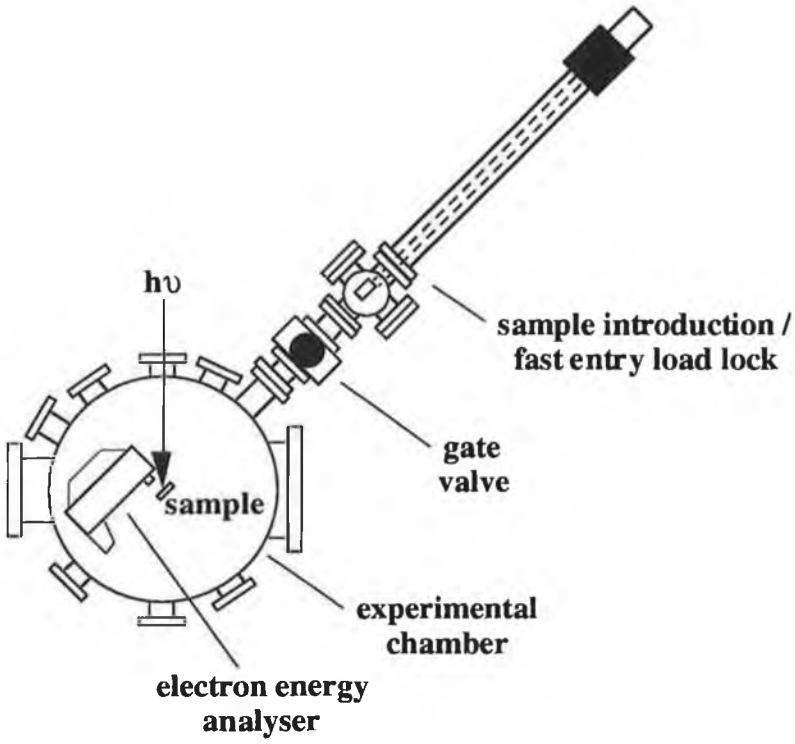

Figure 4.5 Schematic layout of experimental chamber.

The samples once introduced into the main chamber were initially heated slowly, using radiative heating by a filament behind the sample plate, to about 200°C. It was important to heat the sample slowly to ensure the In bond was not disturbed. The arsenic overlayer was then thermally desorbed from the GaAs samples by e-beam heating to 350°C leaving a highly ordered arsenic rich reconstructed surface. This was observed to have a (2x2) reconstruction using LEED.

4.4.3 Sample Passivation.

Sulphur passivation was carried out in the main chamber using a beam of molecular sulphur provided by an electrochemical cell. The sulphur flux was generated by the decomposition of Ag_2S when an EMF was applied to the heated electrochemical cell illustrated in figure 4.5 [9-11]. The pellet for the cell, about 10 mm in diameter and length, was made by pressing powders of silver, silver iodide and silver sulphide together with a sheet of platinum mesh in a pellet press under a force of 1 tonne. A silver foil disc placed next to the fused silver powder provided electrical contact for the silver iodide cathode while the platinum mesh made contact with the silver sulphide anode. The cell was then fitted into a glass tube, one end of which had a 40 mm long capillary with a 5 mm inside diameter orifice through which the sulphur diffused. External

electrical contact from the anode and cathode was made via platinum leads. pressure contact was maintained on the cell by means of a glass piston which was secured to the tube using steel springs. A sheet of stainless steel together with several windings of tungsten wire provided uniform heating of the electrolyte array, the temperature of which was monitored by a thermocouple. The entire cell was mounted on a $2^3/_4$" flange thus providing a vacuum compatible sulphur source.

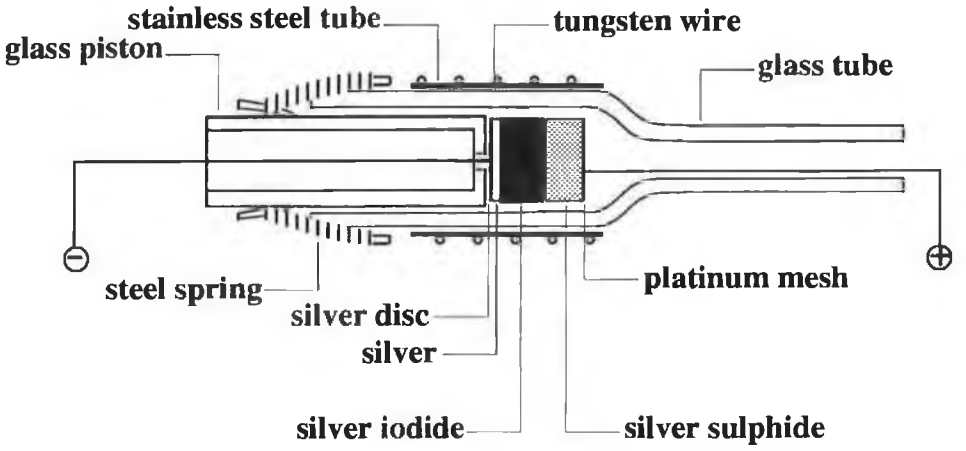

Figure 4.6 Schematic diagram of the sulphur cell after Roberts [8].

The cell operates on the principle that at high temperatures (~300°C) the cell becomes active due to changes in the chemical potential. Since silver iodide is an ionic conductor it acts as a source to the silver ions and attracts them from the silver sulphide to the silver, realising sulphur molecules at the front of the cell.

4.4.4 Data Acquisition.

As described in section 4.4.2 the sample was heated to 350°C to desorb the arsenic cap. Following this, LEED was carried out on the sample and a clear (2x2) LEED pattern was observed. Using the LEED spots as reference, the sample was aligned with either the $\overline{\Gamma}\overline{M}$, $\overline{\Gamma}\overline{M}'$ or $\overline{\Gamma}\overline{K}$ direction parallel to the plane of polarisation of the synchrotron light. The analyser was rotated from -25° to 71° (with respect to the surface normal) in 2° steps at photon energies of 20 eV, 24 eV and 28 eV. All scans were recorded with the photon beam making an angle of 45° to the sample normal. The system resolution was approximately 350 meV. The work function was ~5 eV. Normal emission scans at a series of photon energies were also recorded. The sample was then exposed to a sulphur flux for about 3 minutes. After the sulphur deposition a (1x1) LEED

pattern was observed. The same scans as above were repeated along the symmetry directions.

Throughout the experiment Fermi edge scans were recorded frequently to act as a reference, so any energy drift in the photon energy or change in the valence band edge could be determined. Typical data sets obtained are shown on the following pages. The valence band scans for the GaAs(111)B surface in the $\overline{\Gamma}\overline{M}'$ direction at 28 eV and for the sulphur treated surface also in the $\overline{\Gamma}\overline{M}'$ direction at 28 eV are shown in figures 4.7 (a) and 4.7 (b) respectively. The dispersion of the bands can be observed. It is also possible to see the reduced number of states on the sulphur passivated surface.

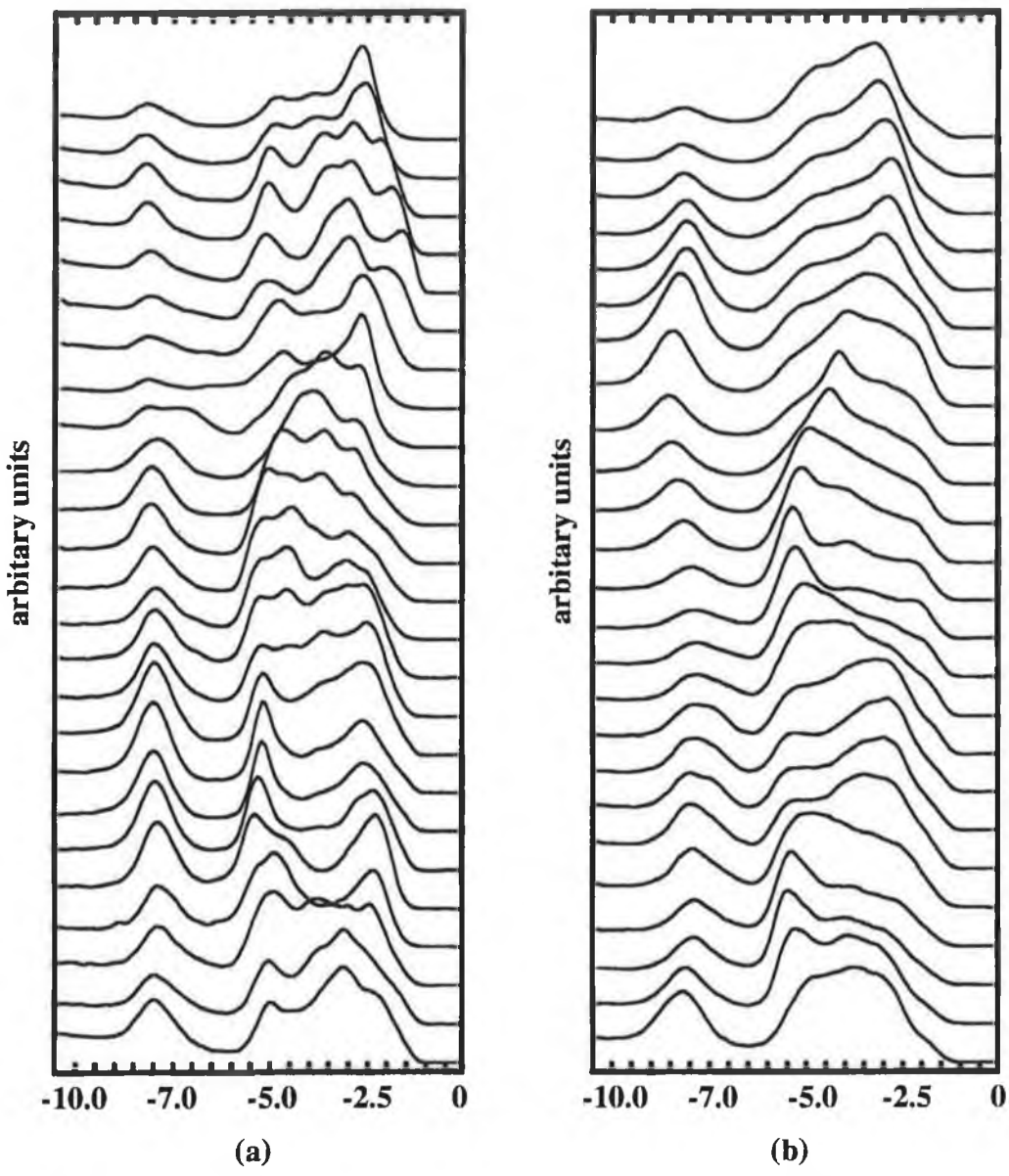

Figure 4.7 Valence band scans for the GaAs(111)B (a) clean surface and (b) sulphur treated surface in the $\bar{\Gamma}\bar{M}'$ direction at 28 eV.

4.5 Data Analysis.

In order to get from kinetic energy (E_K) versus intensity scans to a plot of $k_{||}$ versus binding energy (E_B) it was necessary to identify all peaks in each scan and the energy at which they occurred. To calculate the position in k space of each peak chosen, the momentum (k) was calculated from equation (4.4). The position for each peak in binding energy was calculated from equation (4.3). Once E_B was known it was possible to calculate $k_{||}$ using equation (4.5). By plotting all values of $k_{||}$ versus E_B a map of the electronic band structure for each symmetry direction was compiled. These results are presented on the following pages.

4.6 Discussion.

Examination of the two data sets in figures 4.7 (a) and 4.7 (b) reveals that there are more strong features in both the clean and sulphur treated GaAs than can be explained by bulk initial states alone and that the two surfaces have different electronic properties. This difference is also observed in the $k_{||}$ versus E_B plots.

In order to identify surface states, it is required that $k_{||}$ dispersion is independent of photon energy and that a symmetric dispersion occurs about high symmetry points of the surface Brillouin zone i.e. $\overline{K}$, $\overline{M}$ and $\overline{M}'$. These indications may be observed from the experimental data. For a rigorous analysis it is also necessary to carry out a band structure calculation and project the surface states on it. Band structure calculations were not carried out as part of this thesis and are being done elsewhereby A.A Cafolla and R Whittle.

We will first examine the results for the clean GaAs(111)B. Vertical lines at the (1x1) symmetry points have been drawn in figures 4.8 (a), 4.9 (a) and 4.10 (a). There appear to be 3 or 4 energy bands within 5 eV of the Fermi edge. The first of these disperses up from -3 eV at $\overline{M}'$ to -2 eV at $\overline{\Gamma}$ down to -3 eV at $\overline{M}$ and appears to approach -2 eV again at $\overline{\Gamma}$. It is symmetrical about $\overline{\Gamma}$, $\overline{M}'$ and $\overline{M}$. The second one disperses from about -4 eV at $\overline{M}$ down to about -4.5 eV and back to -4 eV at $\overline{\Gamma}$. It's frequency is twice that of the first. The third band disperses slightly about -5 eV to -5,5 eV with the same frequency as the first band. The fourth band is not very clear but is symmetrical about $\overline{\Gamma}$ at -2.8 eV. There is also a band at -8 eV. This is probably due to transitions from the bulk bands which have been folded back into the (2x2) surface Brillouin zone. For a more detailed analysis band structure calculations would be necessary.

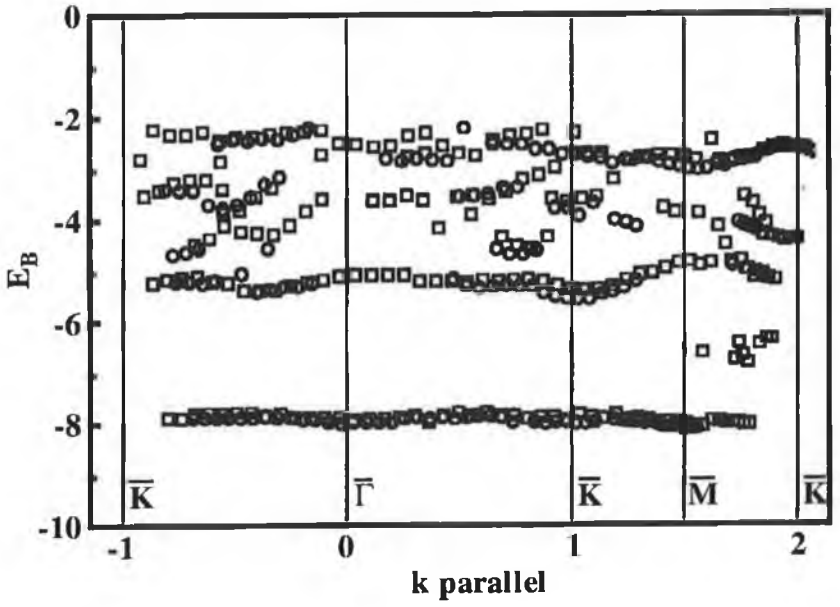

(a)

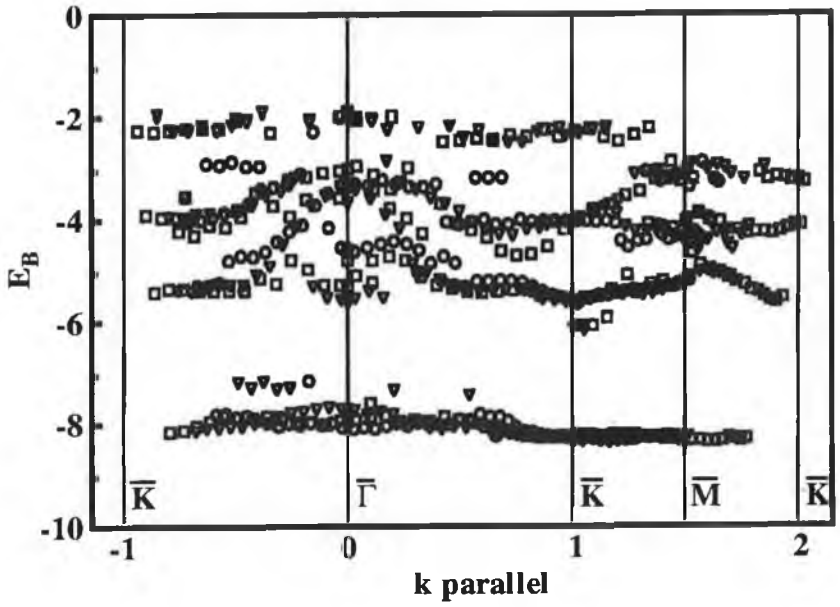

(b)

Figure 4.8 $k_{||}$ vs binding energy for the (a) clean and (b) sulphur treated GaAs(111)B in the $\bar{\Gamma}\bar{K}$ direction.

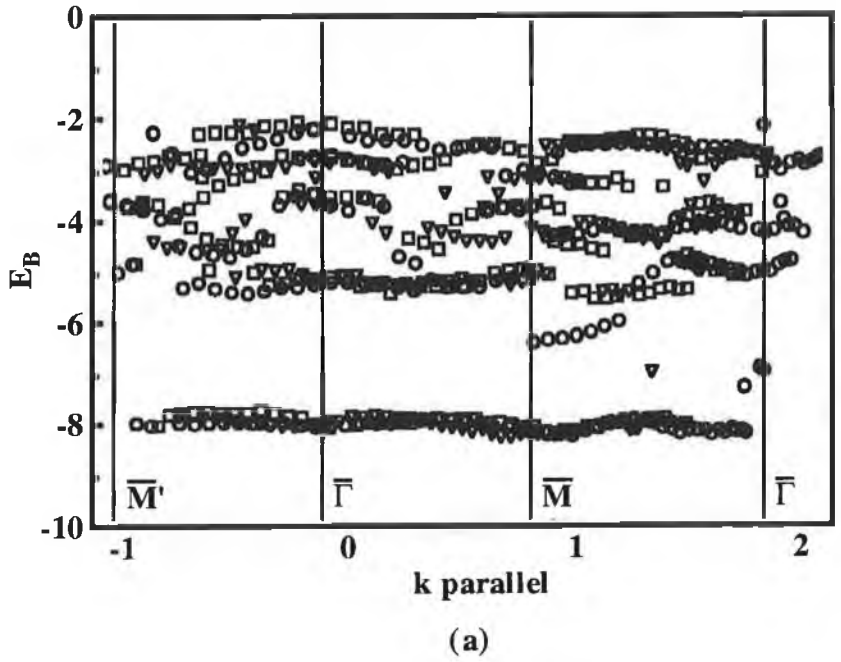

(a)

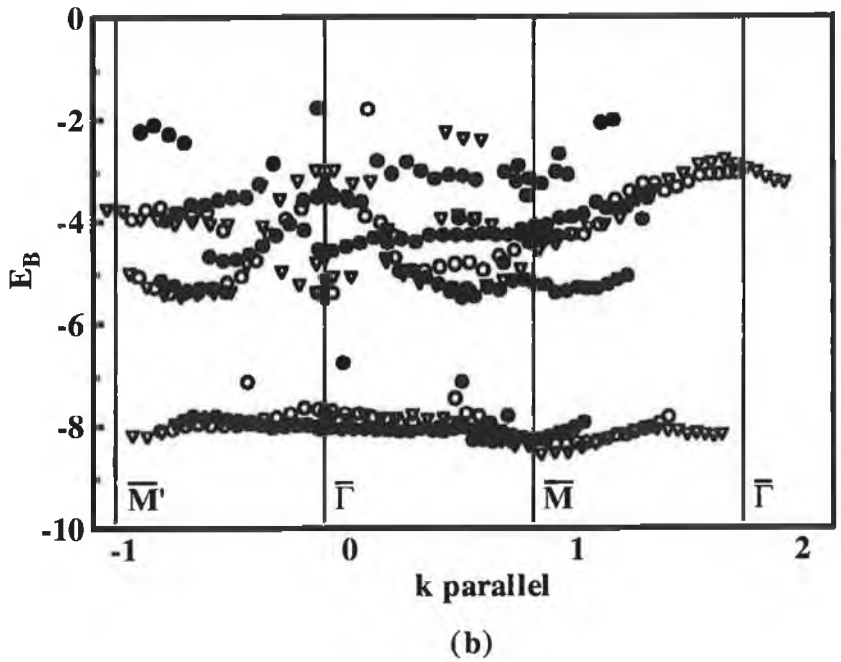

(b)

Figure 4.9 $k_{||}$ vs binding energy for the (a) clean and (b) sulphur treated GaAs(111)B in the $\bar{\Gamma}\bar{M}$ direction.

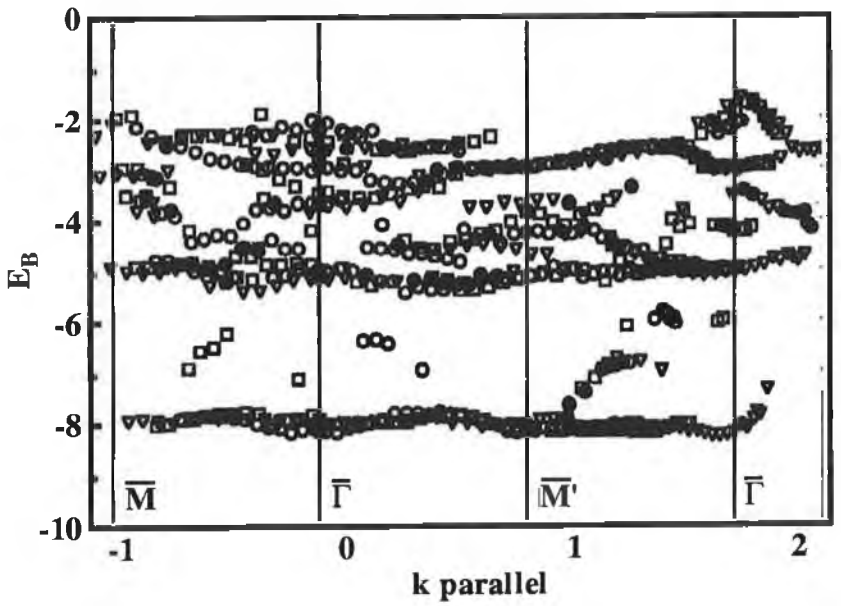

(a)

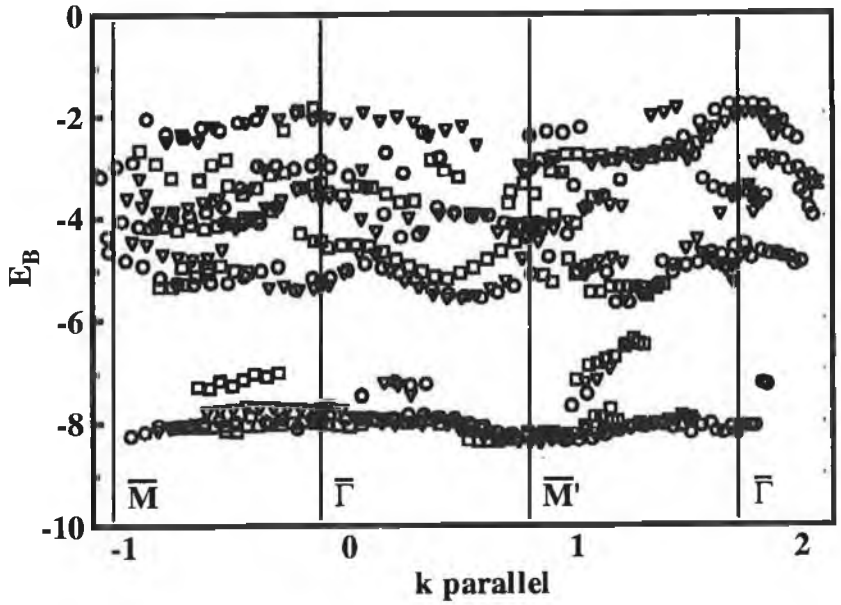

(b)

Figure 4.10 $k_{||}$ vs binding energy for the (a) clean and (b) sulphur treated GaAs(111)B in the $\bar{\Gamma}\bar{M}'$ direction.

In contrast with the clean surface the features on the sulphur treated surface plots (figures 4.8 (b), 4.9 (b) and 4.10 (b)) are not as distinctive. This is probably due to a disordered layer of sulphur on the GaAs surface. The (1x1) LEED pattern observed was probably due to the underlying ordered bulk structure. There appears to be some change in the electronic features which is consistent with passivation. Only three band states can be observed in the S-GaAs surface, at -2 eV, -4 eV and at -5 eV. In the $\overline{\Gamma}\overline{M}$ direction the -3 eV band is completely gone. There is no detailed information available from the S-passivated surface due to the disorder.

Scanning tunnelling microscopy studies [12,13] have shown that large areas of disordered sulphur exist on the surface. While the data presented does not show that sulphur completely passivates the (111)B surface it is clear that changes have occurred to the surface electronic structure and that some surface states have been either been altered or removed by the S overlayer.

4.7 Conclusion.

The results presented in this chapter show the band structure of the clean (2x2) reconstructed GaAs(111)B surface. There is clearly symmetry about the Brillouin zone points on the clean surface. This data provides valuable information on the band structure of the GaAs(111)B. The data show that sulphur deposition has a major effect on the GaAs(111)B surface. There is clearly a chemical interaction between the sulphur and the GaAs. It is clear from this study that sulphur has a major role to play in passivating the (111)B surface. By reducing the quantity of sulphur reaching the sample surface it may be possible to achieve a more ordered surface and thus carry out further studies in this area. There is also the possibility that antimony or selenium or other group 6 elements may passivate the (111)B surface. This would be another possible avenue to follow. To carry out a similar study on the GaAs(111)A surface would also be very informative.

References.

[1] R.D. Briggans and R.Z. Bachrach, Phys. Rev. Lett. **53**(20) (1984) p.1954.

[2] Grown by D.A. Woolf, University of Wales College of Cardiff, Wales.

[3] A. Kahn, Surf. Sci. Rep. **3** (1983) p.193.

[4] R.M. Feenstra, J.A. Stroscio, J. Tersoff and A.P. Fein, Phys Rev Lett. **58** (1987) p.1192.

[5] G.V. Hansson and R. Uhrberg, Surf. Sci. Rep. **9** (1988) p.197.

[6] E.W. Plummer and W. Eberhardt in Advances in Chemical Physics **49** (1982) p.533.

[7] T.S. Turner and D. Teehan, Technical Memorandum Daresbury Laboratory, (1992).

[8] L. Roberts , PhD. Thesis ,(1993).

[9] W. Heegeman, K.H. Meister, E. Bechtold and K. Hayek, Surf. Sci. **49** (1975) p.161.

[10] C. Wagner, J. Chem. Phys. **21** (1953)p.1819.

[11] G.J. Davies, D.A. Andrews and J. Heckingbottom, J. Appl. Phys. **52** (1981) p.7214.

[12] B. Murphy, P. Moriarty, L. Roberts, A.A. Cafolla, G. Hughes, L. Koenders and P. Bailey, Surf. Sci. Accepted May 1994.

[13] P. Moriarty, B. Murphy, L. Roberts, A.A. Cafolla, G. Hughes, L. Koenders and P. Bailey, Surf. Sci. submitted.

growth of transition metal dichalogenides [9], it has not been established whether the sulphur treatment leads to an electronic passivation of the surface as defined above. There has been a debate in the literature as to whether the improvement in the electronic characterisation of the GaAs surface displayed by sulphur treatment is due to an increase [10-12] or decrease [13] in the surface band bending. However, there is an increasing consensus amongst more recent studies that, at least for the GaAs(100) surface, both sulphur [14] and selenium [15,16] terminated surfaces display significant reductions in the surface band bending. This latter result is in keeping with the reported increased dependence of Schottky barrier height on metal work function for the $(NH_4)_2S_x$ treated GaAs(100) surface [3].

The theoretical predictions of Ohno [6] suggested that the formation of a sulphur terminated GaAs(111)A surface would result in a dramatic reduction of the intrinsic mid-gap surface state density and a shift of the Fermi level towards the valence band maximum (VBM), for n-type materials, due to the presence of sulphur induced surface states further down the bandgap. this would of course result in an increase in band bending at the surface. The results of the calculations for sulphur adsorbed on the (111)B surface did not favour an exchange between the sulphur and the top As layer, nor did they predict any change in the Fermi level position. In order to determine whether the clean surface density has been altered by the adsorption of a sulphur overlayer, it is necessary to know the original position of the Fermi level relative to the band edges and to monitor changes in this position with Sulphur adsorption. In this study monitoring was accomplished by undertaking a high resolution surface sensitive core level photoemission study of the interactions of sulphur with the (2x2) reconstructed GaAs(111)A and (111)B surfaces using a synchrotron radiation source. This technique displays a high sensitivity to the chemical interactions at the surface and changes in the binding energy of the core levels, with respect to a fixed reference metallic Fermi level, are indicative of alterations in the surface band bending. The clean surfaces were prepared by thermally desorbing a protective As overlayer which had been deposited following molecular beam epitaxy (MBE) growth in a separate chamber [17]. This experimental procedure allows the clean surface to be fully characterised prior to the in situ deposition of a sulphur overlayer. Changes in the Fermi level position can therefore be directly correlated with surface chemical bonding. In a separate chamber, an ultra high vacuum scanning tunnelling microscopy (UHV-STM) was used to

investigate the structure of the sulphur treated GaAs(111)B surface. The results presented in this paper display significant differences between an in-situ UHV study of the interaction of sulphur with both of these orientations of the GaAs(111) surface and the previous wet chemically prepared surface studies [1].

5.2 Experimental .

5.2.1 The Beam Line.

The experiments were carried out at station 6.1 at Daresbury synchrotron radiation source in the UK. At Beam line 6.1 monochromatic light of energy 20 to 280 eV from the synchrotron was delivered into an electron energy spectrometer equipped to perform solid state photoemission for surface science. A schematic diagram of the beam line optics is shown in figure 5.1 shown below. A pre-mirror deflected synchrotron light horizontally through an angle of 11.4° onto a plane grating. The dispersed light was then focused vertically through exit slits by one of two spherical mirrors. These two mirrors provided four energy ranges as there were two focus positions for each mirror. After the exit slits, an ellipsoidal focusing mirror deflected the light horizontally through 10° to bring it to a focus at the centre of the experimental chamber. The wavelength (energy) of the monochromatic light was selected by rotating the grating about its horizontal axis. The photon energy used was 100 eV to investigate the As 3d and the Ga 3d core levels. The S 2p core levels were studied with a photon energy of 190 eV.

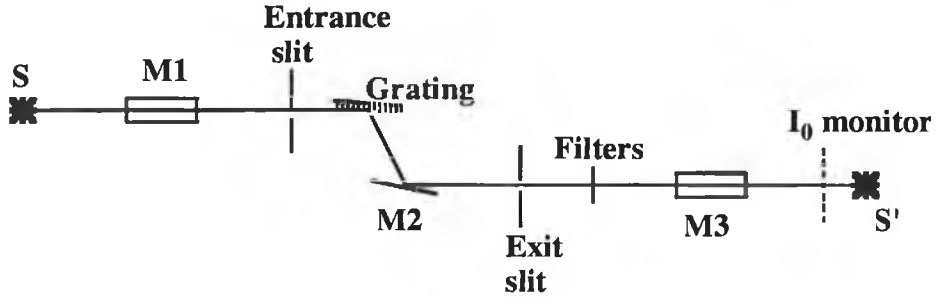

Figure 5.1 Schematic layout of beam line 6.1 optics.

The main experimental chamber was a non magnetic μ metal chamber pumped by a turbomolecular pump a titanium sublimation pump and an ion pump. The base pressure in the chamber after bakeout was $1x10^{-10}$ mbar. The samples were introduced to the main chamber by a linear transfer mechanism via a fast entry load lock.

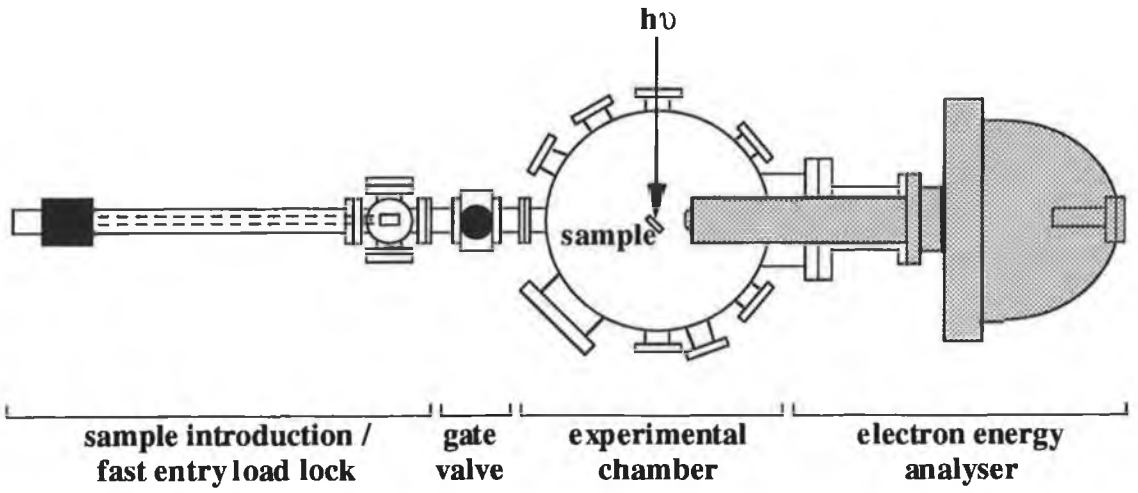

Figure 5.2 Schematic layout of experimental chamber.

5.2.2 Sample Preparation and Manipulation.

The samples used were MBE grown GaAs epi-layers doped with silicon atoms to $1x10^{18}$ cm^{-3} and subsequently capped in situ with a protective arsenic layer [17]. The GaAs samples were cleaved from wafers to approximately 10 mm x 5 mm. Each sample was mounted on a molybdenum sample spade with molten indium as described in section 4.4.2. The spade and sample were then mounted on a carousel type holder in the introduction lock. Once the sample was transferred to the main chamber a wobble stick was used to withdraw the sample spade from the carousel and slide it into the holder at the end of the manipulator. While both the GaAs(111)A-Ga terminated and (111)B-As terminated surfaces display the same (2x2) LEED surface reconstruction, the corresponding surface geometries are significantly different. The reconstruction for the GaAs(111)B illustrated in figure 4.1 consists of an As trimer arrangement while the reconstruction for the (111)A is due to Ga vacancies (figure 5.3).

The As 3d and Ga 3d core levels were studied for the clean GaAs surface. Then the molecular sulphur was introduced on to the samples using an electrochemical sulphur cell [18-21], as described in section 4.4.3. The samples were exposed to a diffuse sulphur flux for 10 minutes. A diffuse (1x1) LEED pattern was observed indicating that a disordered overlayer of sulphur a few angstroms thick was present. This was confirmed using Auger spectroscopy and photoemission. The As 3d, Ga 3d and S 2p core levels were studied for the sulphur treated surface at room temperature and after a series of anneals from 150°C to 580°C.

Valance band maxima were also recorded for each anneal.

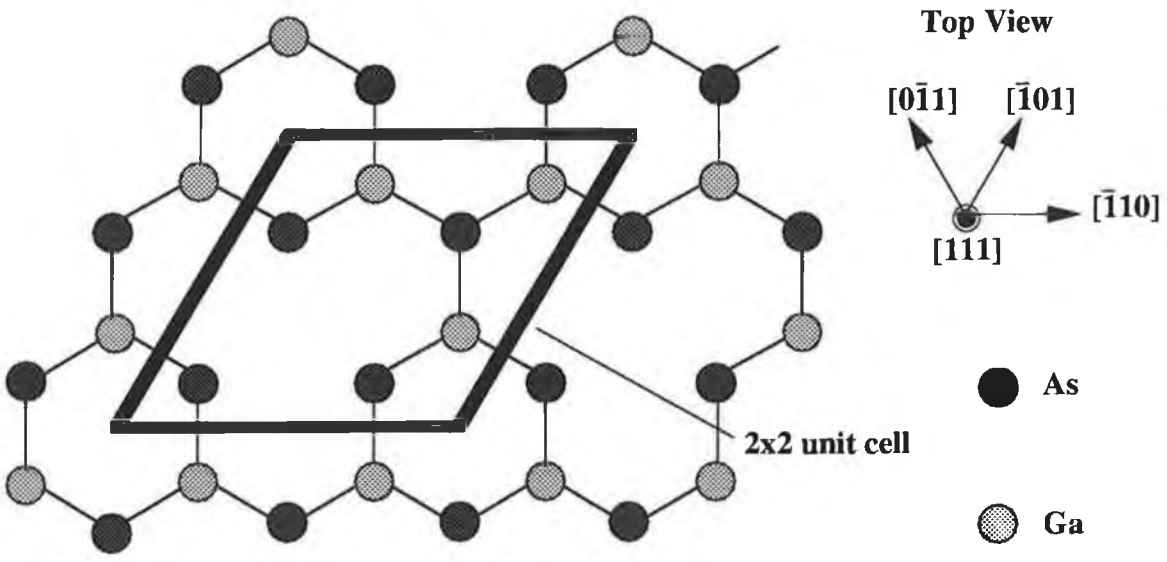

Figure 5.3 A top view of the (2x2) reconstructed GaAs(111)A surface. The reconstruction arises from an ordered array of Ga vacancies.

5.3 Analysis techniques.

In order to obtain precise values for core level binding energies as well as the chemically shifted As and Ga components, it was necessary to curve fit the raw photo emission data. The core level spectra were fitted using a non-linear least squares analysis fitting programme [22] written by A.A. Cafolla. This was carried out assuming a Voigt profile: a Lorentzian convoluted with a Gaussian line shape. The Lorentzian line shape describes the statistical broadening of a core level and the Gaussian distribution reflects the instrumental resolution. The other parameters included the spin orbit splitting of the As and Ga 3d core levels, the relative intensities or branching ratio of the spin orbit split components and the surface core level shifts due to the displacement of surface atoms from the bulk atoms. The background was fitted with a third order polynomial. The fitting parameters are given in table 5.1 below.

The Lorentzian, the spin orbit split and the branching ratios were kept constant to 0.01 eV. The Gaussian was allowed to vary ±0.03 eV. These values are consistent with previously published values.

	As 3d (eV)	Ga 3d (eV)
Lorentzian	0.14	0.14
Gaussian	0.49	0.45
Spin Orbit Split	0.7	0.46
Branching Ratio	0.65	0.65
Surface Core Level Shift	-0.5	

Table 5.1 Fit parameters.

5.4 Results.

5.4.1 GaAs(111)A.

Photoemission spectra of the clean Ga 3d and As 3d core level peaks for the GaAs(111)A surface are shown in figures 5.4 and 5.5 respectively. The (2x2) reconstruction observed on this surface is believed to be caused by the creation of Ga vacancies in the ideal (1x1) Ga terminating layer [23,24]. This allows the top Ga layer to compress towards the underlying As layer adopting a local bonding configuration similar to the atomic structure on the cleaved GaAs(110) surface [25]. This structural model results in the formation of six fold rings of alternate Ga and As atoms between which charge transfer can occur resulting in empty Ga dangling bonds and filled As dangling bonds at the surface. This surface would therefore be expected to result in the observation of surface core level shifted (SCLS) components similar to those reported on the GaAs(110) surface [26]. While there is clear evidence, following curve fitting, of a SCLS component shifted by 0.4 eV to higher binding energy on the Ga 3d, consistent with charge donation, no corresponding SCLS on the As 3d indicative of charge acceptance is observed.

Following the room temperature (RT) deposition of 1-2 monolayers of sulphur from the electrochemical cell, there is evidence of chemical interaction between sulphur and both the Ga 3d and As 3d core levels as seen in Figures 5.4 and 5.5 respectively. This is accompanied by the disappearance of the clean (2x2) surface reconstruction which is replaced with a (1x1) LEED pattern with a high diffuse background and broad spots. The Ga 3d peak consistently required two chemically components, shifted by 0.4 and 0.9 eV towards higher binding energy in addition to the bulk peak. While it is difficult to distinguish the 0.4 eV chemically shifted component from the SCLS for RT sulphur adsorption, it could be argued that a sulphur coverage sufficient to

remove the clean (2x2) surface reconstruction would also be expected to attenuate the SCLS component. In addition, the fact that the intensity of the 0.4 eV shifted component increases in intensity with annealing supports the assumption that it is a chemically shifted component not a residual SCLS component.

One very broad chemically shifted component (FWHM = 1.2 eV) on the As 3d, shifted by 1.2 eV towards higher binding, is evidence of strong As-S interaction and possibly the formation of a disordered arsenic sulphide layers which has been proposed for the sulphur-GaAs(100) surface interaction [27]. The significantly larger intensity of the chemically shifted component on the As 3d compared with the Ga 3d is consistent with the reported interaction of sulphur with the GaAs(100) surface, even when this surface is in a Ga rich reconstruction [14,18]. Figure 5.4 shows that the intensity of the chemically shifted components on the Ga 3d core level increases as a function of annealing temperature. While the intensity of the 0.4 eV chemically shifted component increases from 26% of the bulk peak intensity, following RT sulphur deposition, to 35% during the annealing to 450°C, the intensity of the 0.9 eV chemically shifted component increases from 8% of the bulk peak intensity to 27% over the same temperature range. The (1x1) LEED pattern which appears following RT sulphur deposition becomes increasing well defined with a substantial decrease in the diffuse background as the sample was annealed.

The evolution of the As 3d core level as a function of annealing temperature, shown in figure 5.5 illustrates the attenuation in the intensity of the chemically shifted component. This component is completely removed from the spectrum at an annealing temperature of 350°C where the As 3d peak can be fitted with one spin-orbit split component which remains the case, even when the sulphur has been desorbed at 550°C and the (2x2) surface reconstruction has been restored. The general form of this interaction agrees with previous reported studies [4]. Photoemission spectra of the S 2p core level in figure 5.6 clearly show two distinct chemically shifted components, even above an annealing temperature of 350°C. At these annealing temperatures, there is no evidence of As-S bonding. Therefore, the two S 2p components must correspond to sulphur in two different chemical environments at the surface, but only bonded to Ga atoms. Upon annealing, the relative intensity of these two components change with the higher binding energy component (binding energy = 161.5 eV with respect to the VBM) increasing in magnitude with respect to the lower

energy component, while the energy separation between the components remains constant at 0.7 eV. It is not likely that these components correspond to Ga-S and S-S surface bonds following the work of Sugahara *et al.* [28] which showed that the binding energy of the S-S bonding component was approximately 2 eV shifted to higher binding energy with respect to sulphur bonded to either Ga or As.

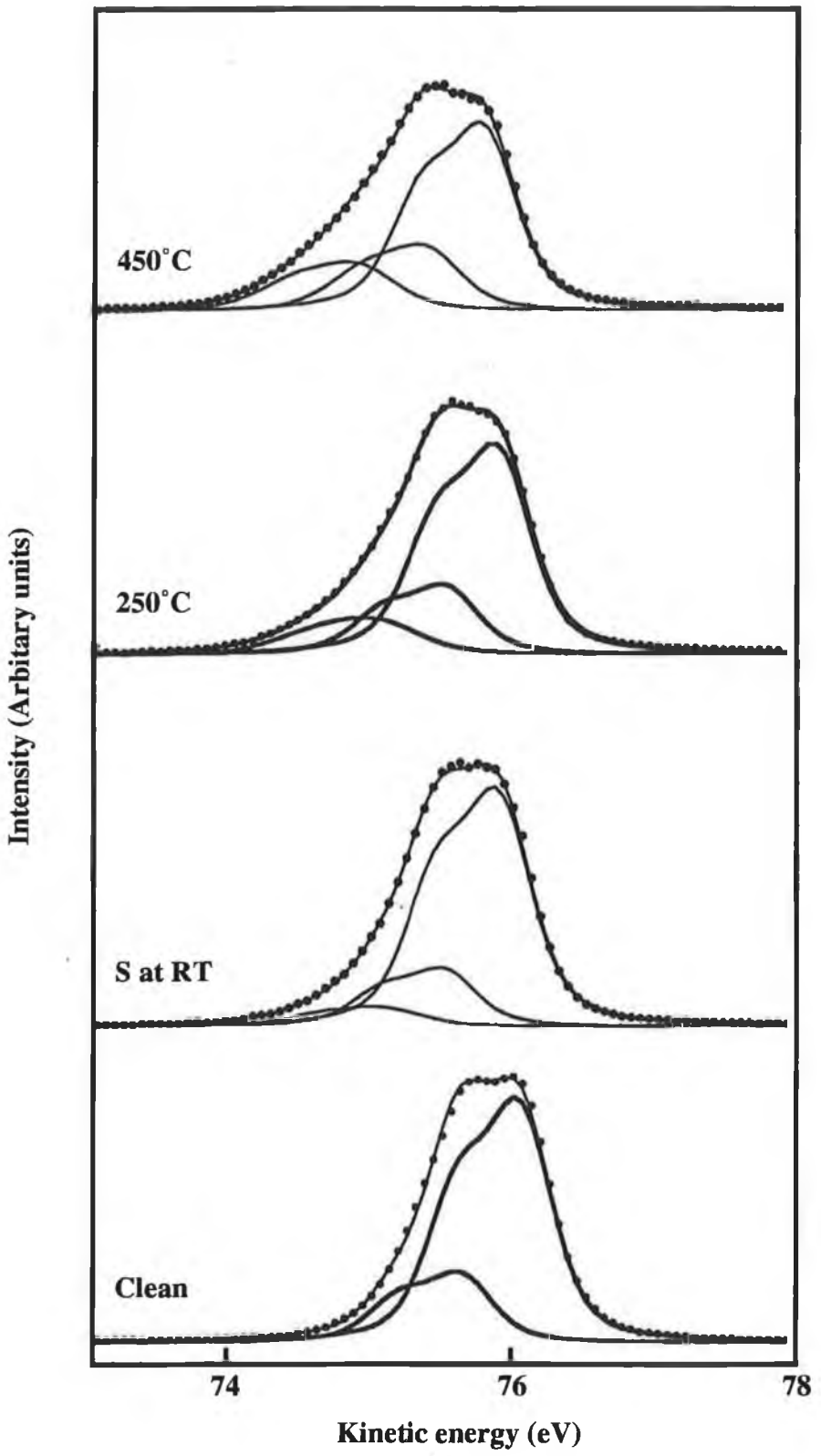

Figure 5.4 Changes induced in the Ga 3d photoemission spectrum of the GaAs(111)A surface as a function of sulphur deposition and annealing. Photon energy=100eV.

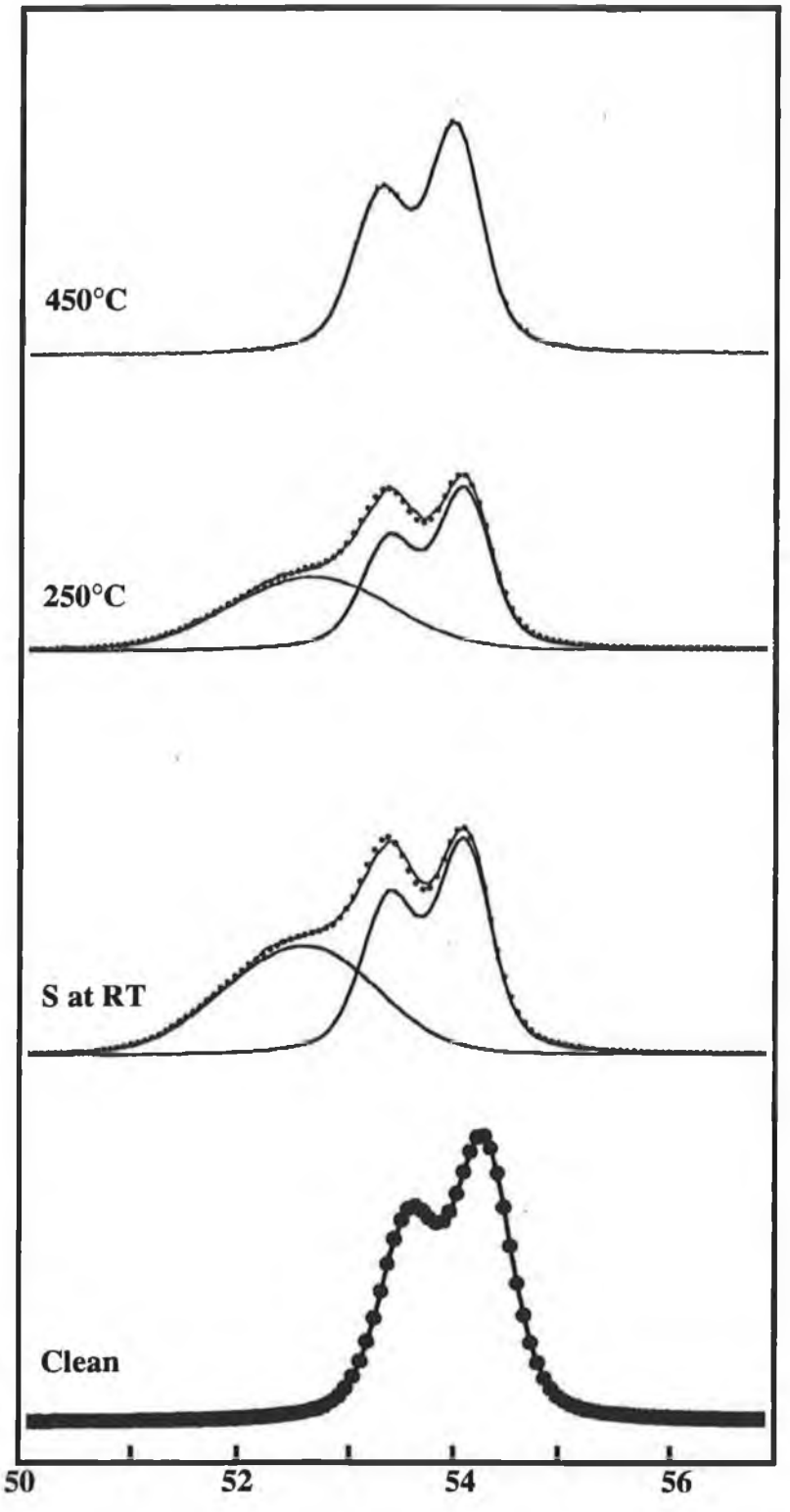

Figure 5.5 Changes induced in the As 3d photoemission spectrum of the GaAs(111)A surface as a function of sulphur deposition and annealing. Photon energy=100eV.

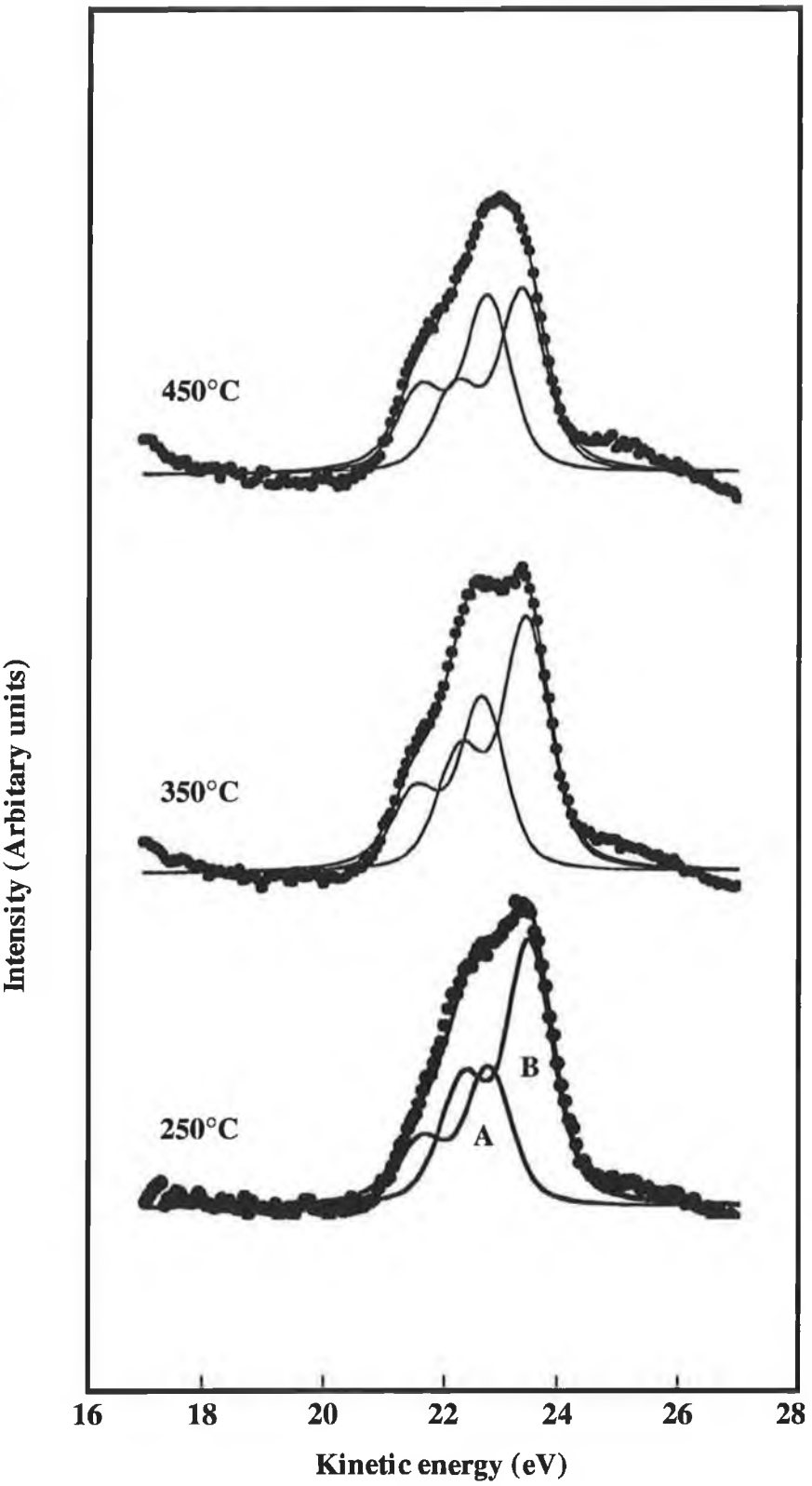

Figure 5.6 Changes induced in the S 2p photoemission spectrum of the S/GaAs(111)A surface as a function of annealing. Photon energy=190eV.

5.4.2 GaAs(111)B.

Figures 5.7 and 5.8 illustrate the photoemission spectra of the Ga and As 3d core levels for the clean GaAs(111)B surface respectively. As previous photoemission studies have reported [29,30], the Ga 3d peak can be fitted with a single spin-orbit split component. This indicates that the (2x2) surface reconstruction of this surface results in all the Ga atoms occupying four-fold bulk co-ordinated sites, consistent with the proposed model of arsenic trimers chemisorbed on top of the bulk As terminated layer. Again, consistent with previous photoemission studies [29,30], three components are necessary to fit the As 3d peak, the bulk component and two SCLS components labelled S_1 and S_2 in figure 5.8. The component shifted to relative higher binding energy, S_1, has been attributed to the As atoms chemisorbed on to the As terminated surface in the trimer bonding formation which creates the (2x2) surface symmetry [32].

The changes in the Ga 3d core level following RT sulphur deposition and annealing are also illustrated in figure 5.7. It is difficult to distinctly resolve a chemically shifted component for RT adsorption, the peak only broadens, which is consistent with the double As terminating layer of the (2x2) reconstruction. The evolution of the Ga 3d with annealing is similar to that observed for the (111)A surface, displaying an increasing Ga-S bonding interaction. However, in this case, the 0.5 eV chemically shifted component can best be fitted with a broadened Gaussian which continued to increase both in width (to a FWHM 0.75 eV) and in intensity up to an annealing temperature of 500°C. At this temperature, the ratio of the intensities of the chemically shifted component to bulk component for the Ga 3d peak approached 0.85. This ratio is much larger than would be expected for a one monolayer adsorbed coverage [33]. The (2x2) clean surface LEED pattern was replaced by a diffuse (1x1) pattern following RT sulphur adsorption. This (1x1) pattern became increasingly well resolved as a function of annealing until at 500°C it displayed sharp spots with very low background. An annealing temperature of 580°C was required to desorb sulphur from this surface which then exhibited a weak (1x1) LEED pattern with high background.

Figure 5.8 illustrates the evolution of the As 3d core level following sulphur deposition and annealing. It can be seen that for RT adsorption, both surface components S_1 and S_2 of the clean surface spectrum are required in order to accurately fit the peak. There is a broadening of the S_1 component which increases in intensity with respect to the bulk

peak, however, the S_2 component remains a feature of the spectrum although somewhat attenuated in intensity. A fourth broad component (FWHM 0.8 eV) shifted by 1.2 eV to higher binding energy also appears. These changes are similar to those by Rank *et al.* [30] for the adsorption of H_2S on the GaAs(111)B surface. They also observed the preferential adsorption on As without the disappearance of the S_2 SCLS component. As was observed for the (111)A surface, there is a rapid attenuation in the intensity of the broad chemically shifted component at 1.2 eV higher binding energy during the annealing until at 250°C, this component completely disappears. This is accompanied by a decrease in the intensity of the S_1 component which is completely removed at 500°C. However, it is important to note that the SCLS component labelled S_2 remains a feature of the spectra throughout the annealing sequence and increases to its clean surface intensity, with respect to the bulk peak, following the 500°C anneal. This suggests that there are always As atoms incorporated in the top atomic layer.

The evolution of the S 2p spectrum in the annealing range 300-500°C, illustrated in figure 5.9 shows distinct differences from the behaviour observed on the GaAs(111)A surface. As the annealing temperature approaches 500°C, the spin-orbit split doublet becomes increasingly well resolved. This suggests that the annealing sequence results in the sulphur preferentially occupying one distinct chemical environment at the surface, unlike the interactions on either the (111)A or (100) surfaces.

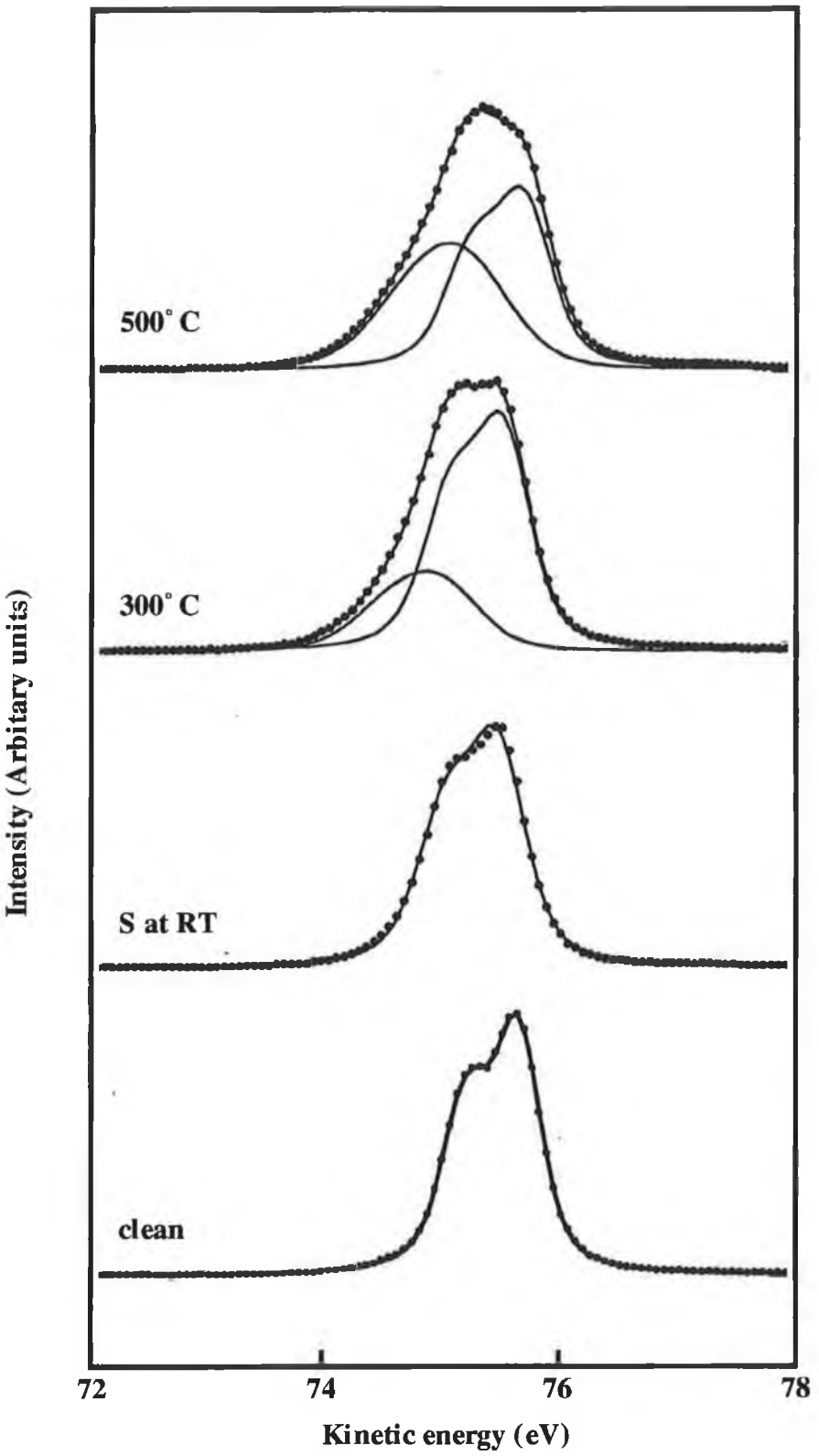

Figure 5.7 Changes induced in the Ga 3d photoemission spectrum of the GaAs(111)B surface as a function of sulphur deposition and annealing. Photon energy =100eV.

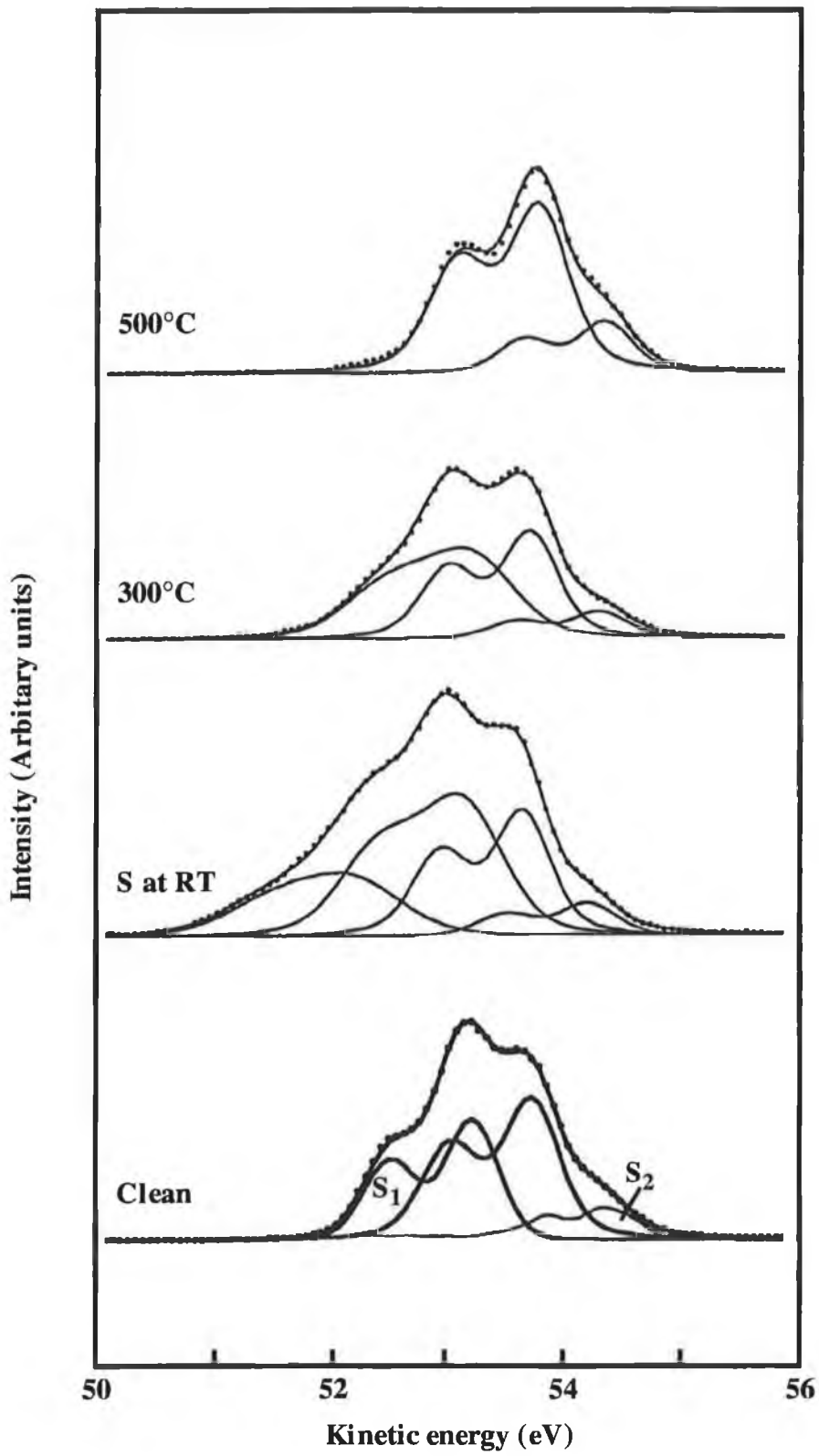

Figure 5.8 Changes induced in the As 3d photoemission spectrum of the GaAs(111)B surface as a function of sulphur deposition and annealing. Photon energy=100eV.

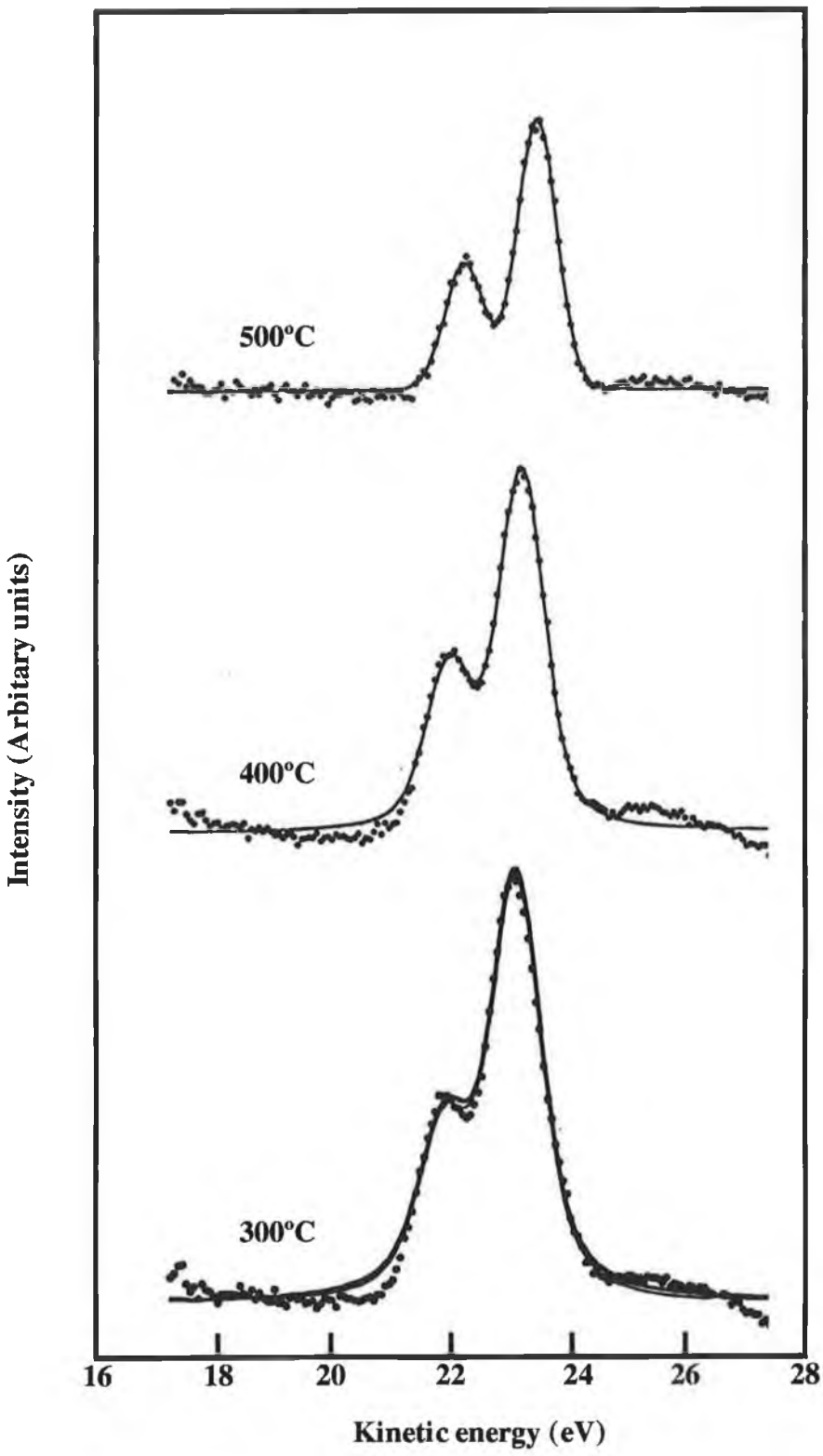

Figure 5.9 Changes induced in the S 2p photoemission spectrum of the S/GaAs(111)B surface as a function of annealing. Photon energy=190eV.

5.4.3 STM Study.

The STM image of the clean decapped GaAs (111)B surface [31] (V_{bias}= 3 V, I = 50 pA) bore a strong resemblance to that reported by Biegelsen *et al.* [24] for an MBE prepared surface with 8 Å spacing between adjacent peaks in the image, consistent with a trimer model surface reconstruction. For RT sulphur adsorption, while the surface exhibited a clean (1x1) LEED pattern, the STM images revealed a disordered surface layer (figure 5.10 (a)). It can be inferred from this that the (1x1) reconstruction is the bulk pattern showing through a disordered surface layer. This is consistent with the very large chemical shift on the As 3d observed for RT adsorption which is indicative of strong chemical interaction and possibly compound formation, similar to the interaction on the GaAs(111)A surface. The STM image of the annealed shown in figure 5.10 (b) clearly shows regions of the surface which are highly ordered, however, this order is not long range. This surface nevertheless exhibited a sharp (1x1) LEED pattern.

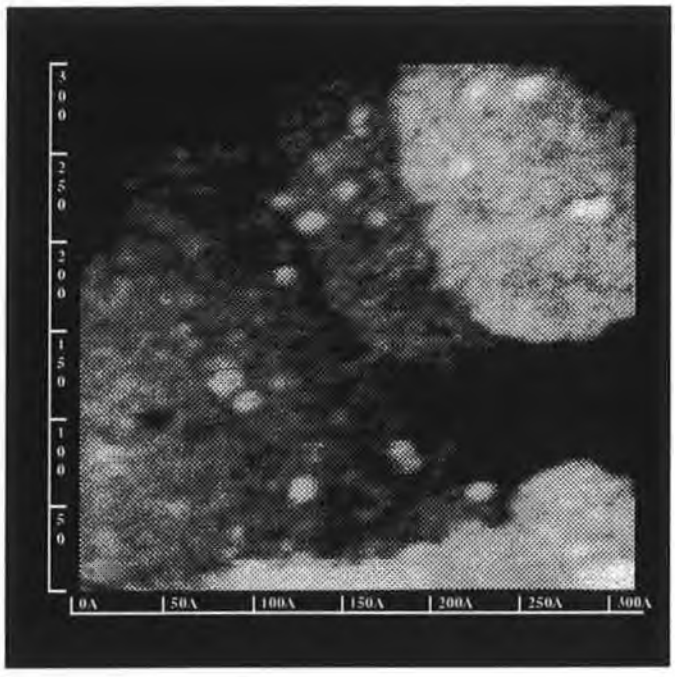

(a)

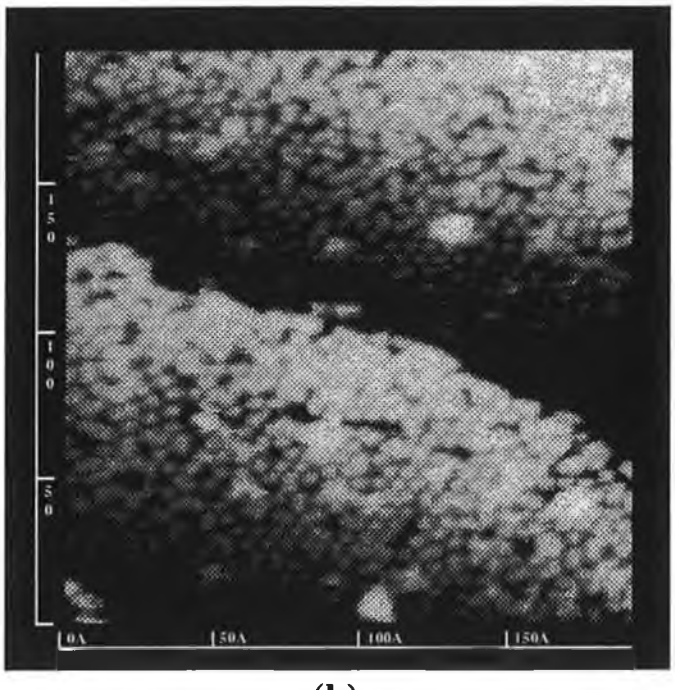

(b)

Figure 5.10 STM images of the GaAs(111)B surface after (a) sulphur deposition and (b) annealing at 450°C

5.5 Discussion.

While there have been many studies of the interaction of sulphur with the various GaAs surfaces, the details of the interaction are still unclear. This may be due to the variety of preparation techniques used. The degree to which sulphur electronically passivates the GaAs surface, in terms of reduction of surface states remains unclear. However, by accurately knowing the Fermi level position on the clean surface prior to deposition, it is possible to determine the effect of sulphur deposition and the subsequent annealing process, which is known to drastically alter the surface chemistry and the surface band bending. It has been recently found [14] for the interaction of sulphur on the GaAs(100) surface, that the degree of Fermi level movement upon annealing depended on the precise Ga/As surface concentration ratio of the initial clean surface reconstruction. This dependence would not be expected for either the GaAs(111)A or (111)B, which both display a single (2x2) reconstruction over a wide temperature range [34].

The results of the study of the interaction of sulphur with the GaAs(111)A surface clearly indicate that the sulphur bonded to Ga atoms after anealing above 350°C exists in two distinct chemical environments. This is in contrast to the result obtained for the wet chemical study by Scimeca *et al.* [4] in which they attributed these two components to evidence of As-S and Ga-S bonding, however, it is in agreement with the observation reported for the interaction of both sulphur [14] and selenium [15,16] with the GaAs(100) surface. From this study it is concluded that the presence of two chemically shifted components on the Ga 3d peak suggests that the Ga atoms are also involved in two distinct chemical environments at the surface. The changes in the intensities of these chemically shifted components, induced by annealing, can be correlated with the two distinct components in the S 2p spectra. By considering the relative change in the magnitude of the two S 2p components with annealing and the relative binding energy, it is proposed that the higher binding energy component (A) can be assigned to bulk co-ordinated sulphur atoms and the lower binding energy component (B) to surface bonded atoms. This suggests that the sulphur atoms which substitute As atoms below the surface act as shallow donors and therefore have a relatively higher binding energy than the sulphur atoms at the surface. The relative increase in the intensity of the component (A) with annealing is consistent with more sulphur atoms being driven into the topmost atomic layers exchanging with bulk co-ordinated As atoms. This can be

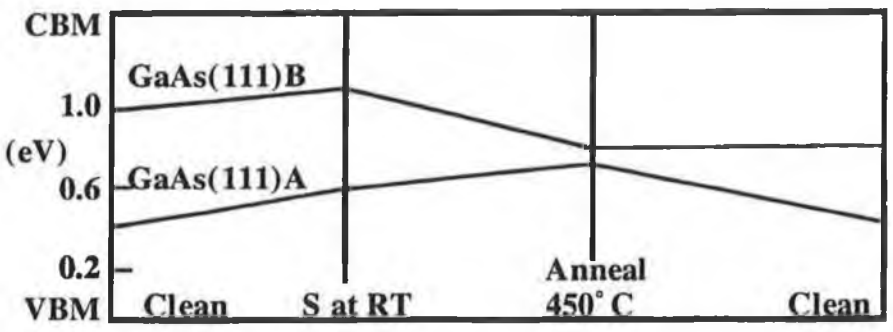

Figure 5.11 Fermi level movements for S/GaAs(111)A and S/GaAs(111)B surfaces for RT sulphur adsorption and annealing.

Figure 5.11 fermi edge movement.

correlated with the increase in the 0.9 eV chemically shifted component on the Ga 3d as a function of annealing which from these results would correspond to Ga atoms being four fold co-ordinated to sulphur near the surface. Attributing the lower binding energy component to the bulk co-ordinated atoms is consistent with the results reported by Maeda *et al.* [34] for the assignment of the two component peaks in the Se 3d spectra for its interaction with the GaAs(100) surface. Above an annealing temperature of 350°C, the As 3d core level can be fitted with one spin-orbit split component indicating that it exists in a bulk-like configuration near the surface. Annealing to 550°C removes any trace of sulphur within the escape depth of both the photoemission and Auger spectroscopy measurements. Scimeca *et al.* [4] reported the results of a secondary ion mass spectroscopy (SIMS) study, which indicated that there was no imbedded sulphur in the GaAs bulk following the high temperature anneal.

The effect of sulphur deposition and subsequent annealing on the position of the Fermi level in the GaAs(111)A band gap is shown in figure 5.11. The Fermi level on the clean surface is 0.45 eV above the VBM and following the RT deposition of sulphur it shifts 0.2 eV towards the conduction band minimum (CBM), a total shift of 0.3 eV towards the flat band condition. This results in the Fermi level residing in a midgap position on the terminated surface. The calculations of Ohno [6] for a sulphur monolayer singly bonded on top of the GaAs(111)A surface suggested that while the intrinsic surface state density was removed, it was replaced by a sulphur derived surface state density closer to the VBM which could re-pin the Fermi level. These results also show that the adsorption of sulphur on this surface is reversible with the clean (2x2) surface reconstruction being restored following sulphur desorption and the Fermi level returning to its original clean surface position. Considering the results of this study in conjunction with the XSW study of Sugiyama *et al.* [5], it suggests that the sulphur is bonded both on top of the first Ga layer and is also replacing some of the As atoms in the top most atomic layers below the surface, however, this termination does not lead to the electronic passivation of the surface since the Fermi level is in a midgap position.

On the (111)B surface, the results of this work differ significantly form those reported by Scimeca *et al.* [4] for the wet chemically prepared surface. For RT adsorption there is no evidence of Ga-S bonding other than a slight broadening of the Ga 3d core level which is consistent with the proposed double layer AS termination of the clean surface.

Above an annealing temperature of 250°C, the sulphur 2p can be fitted with a single spin-orbit split component which is consistent with the surface termination proposed by Sugiyama *et al.* [5] from the XSW study. However, the photoemission evidence that the intensity of the Ga 3d chemically shifted component continues to increase as a function of annealing temperature, while the magnitude of the As 3d SCLS S_2 component remains constant, is inconsistent with the sulphur remaining solely at the surface. The SCLS component on the As 3d can be attributed to As atoms in the top atomic layer of the sulphur annealed surface. This suggests that during the annealing cycles, some of the sulphur atoms at the surface exchange with bulk co-ordinated As atoms which can then terminate the top atomic layer. It is interesting to note that the binding energy of the single S 2p component on the (111)B surface , 161.5 eV with respect to the VBM, is identical to that of the higher binding energy component on the (111)A surface, which was assigned to four-fold bulk co-ordinated sulphur atoms which exchange with As in the topmost atomic layers. Thus it is concluded that for the sulphur annealed (111)B surface, the uppermost atomic layer consists of both As and sulphur atoms bonded in a three-fold co-ordinate configuration to the underlying Ga layer with sulphur also replacing As atoms in bulk-like sites below the surface. The inability to resolve two separate chemically shifted components on the Ga 3d may be due to the fact that the difference in the chemical environment between Ga atoms bonded to three-fold or four-fold co-ordinated sulphur atoms is not as great as the difference between one-fold and four-fold on the (111)A surface. The STM image of this surface indicates no long range order, suggesting that there is no ideal termination of the surface. Therefore it is proposed that the (1x1) LEED pattern observed on this annealed surface is either due to a mixed As and sulphur top layer or is predominantly due to the underlying bulk structure, but not a highly ordered sulphur overlayer.

The graph of the Fermi level position as a function of sulphur treatment for the (111)B surface, also shown in figure 5.11, indicates that there is no significant reduction in the density of states. The Fermi level position on the clean surface at 1.0 eV above VBM moves 0.1 eV towards the CBM following RT sulphur deposition, but the subsequent annealing results in it moving approximately 0.2 eV towards a midgap position with respect to the clean surface position. The considerable degree of surface disorder present on this surface, evident from the STM images, suggests that surface defects may well play a significant role in

determining the final Fermi level position. When the results for the (111)B surface are compared with those of Sugiyama *et al.* [5], it must be remembered that they only annealed the sulphur treated surface to 300°C which is probably not high enough to promote a significant exchange As-S reaction in the layers underlying the surface. It is worth noting that these authors did speculate that sulphur atoms may be present at third layer arsenic sites.

In contrast with the photoemission study of Simeca *et al.* [4] for the (111)B surface, these results suggest that there are very significant structural changes on the (111)B following sulphur treatment. The (2x2) clean surface LEED pattern is removed by RT deposition of sulphur and cannot be restored by thermal annealing. This is probably due to the removal of As atoms from the surface during the thermal annealing cycles which makes the reformation of As surface trimers impossible. A (1x1) clean surface reconstruction has previously been reported for this surface under certain MBE growth conditions [34]. A recent photoemission study by Sugahara *et al.* [28], comparing the ammonium sulphide and UHV preparation of sulphur terminated GaAs(100) surfaces, showed more chemically shifted components on the wet chemically prepared surface, even at elevated temperatures. This suggests that the liquid based interactions are more complex to analyse than the UHV preparation techniques and that care needs to be taken when comparing results obtained by different preparation techniques. This study suggests that at least for UHV preparation techniques, the (111)B surface is not ideally terminated by a sulphur monolayer and is not electronically passivated by sulphur deposition. It also indicates that as the annealing temperature increases towards the desorption temperature of the sulphur the surface chemistry becomes increasingly complex with strong evidence of exchange reactions between the suphur and bulk co-ordinated As atoms in the underlying atomic layers.

The termination of the GaAs(111)A surfaces by sulphur gallium bonds should lead to a reduction in the chemical reactivity of the surface as the S-Ga bond is stronger than the As-Ga bond [35]. This would explain the previously reported [8,9] chemical inertness of this surface. It is of course possible to reduce the density of surface states without totally removing the band bending [36] and this argument could be made for the GaAs(111)A surface where the band bending is reduced by 0.3 eV. However, it cannot apply to the GaAs(111)B surface where the band bending is seen to increase by approximately 0.2 eV on the sulphur treated surface with respect to the clean surface, especially when the

high doping density of the samples used in the experiment ($n = 1x10^{18}$ cm^{-3}) is considered. A chemical passivation of the surface does therefore not necessarily mean that the surfaces are electronically passivated in terms of a sufficient reduction in the density of surface states which result in the removal of band bending. While both electronic and chemical passivation are simultaneously achievable on the GaAs(100) surface for both sulphur [14] and selenium [15,16] terminated surfaces, these results would suggest that this does not appear to be the case for the sulphur treatment of either the GaAs(111)A or (111)B surfaces.

References.

[1] C.J. Sandroff, R.N. Nottenburg, J.C. Bischoff and R. Bhat, Appl. Phys. Lett. **51** (1987) p.33.

[2] J. Fan H. Oigawa and Y. Nannichi, Jpn. Jnl. Appl. Phys. **27** (1988) p.L1331, **27** (1988) p.L2125.

[3] H. Oigawa, J. Fan, Y. Nannichi, H. Sugahara and M. Oshima, Jpn. J. Appl. Phys. **30** (1991) p.L322.

[4] T. Scimeca, Y. Muramatsu, M. Oshima, H. Oigawa and Y. Nannichi, Phys. Rev. B **44** (1991) p.12927.

[5] M. Sugiyama, S. Maymama and M. Oshima, Phys. Rev. B **48** (1993) p. 11037.

[6] T. Ohno, Phys. Rev. B **44** (1991) p.6306.

[7] D.J. Chadi, Springier series in surf. scie. Vol. **24,** (1991) p.532)

[8] H.Oigawa, J. Fan, Y. Nannichi, K. Ando, K. Saiki and A. Koma, Jpn. J. Appl. Phys. **30** (1991) p.l322.

[9] K.Ueno, T. Shimada, K. Saiki and A. Koma, Appl. Phys. Lett. **56** (1990) p.327.

[10] S. Besser and C.R. Helms, Appl. Phys. Lett. **52** (1988) p.1707.

[11] T. Hasegawa, H. Ishii, T. Sawada, T. Saitoh, S. Konoshi, Y. Liu and H. Ohno, J. Vac. Sci. Technol. B **6** (1988) p.1184.

[12] C.J. Spindt, D. Liu, K. Miyano, P.L. Meissner, T.T. Chiang, T. Kendelewicz, I. Lindau and W.E. Spicer, Appl. Phys. Lett. **55** (1989) p.861.

[13] H. Suahara, M. Oshima, H. Oigawa, Shigekawa and Y. Nannichi, ext. Abatracts of the 21st conf. on the Solid State Devices and Materials (the Japan society of Applied Physics, Toko, 1989) p. 547.

[14] P. Moriarty, B. Murphy, L.Roberts, A.A. Cafolla, G. Hughes, L. Koenders and P. Bailey, Surf. Sci. submitted.

[15] S. Takatani, T. Kilawa and M. Nakazawa, Phys Rev. B **45** (1992) p.10201.

[16] T. Scimeca, Y. Watanabe,R. Berrigan and M. Oshima, Phys. Rev. B **46** (1992) p.10201.

[17] As capped samples were provided by Dr. David Woolf from University colledge Cardiff, Wales.

[18] L. Roberts, G. Hughes, B. Fenema and M Carbery, J. Vac. Sci. Technol. B **10** (1992) p.1862.

[19] W. Heegeman, K.H. Meister, E. Bechtold and K. Hayek, Surf. Sci. **49** (1975) p.161.

[20] C. Wagner, J. Chem. Phys. **21** (1953)p.1819.

[21] G.J. Davies, D.A. Andrews and J. Heckingbottom, J. Appl. Phys. **52** (1981) p.7214.

[22] J.J. Joyce, M. Del Giudice, and J.H. Weaver, Jnl. Electron Spectroscopy and Related Phenomena, **49** (1989) p.31.

[23] S.Y. Tong, G. Xu, W. N. Mei, Phys. Rev. Lett. **52** (1984) p.1693.

[24] K.W. Haberern and M.D. Pashley, Phys. Rev. B **41** (1990) p.3266.

[25] D.J Chadi, Phys. Rev. Lett. **52** (1984) p.1911.

[26] D.E. Eastman T.C. Chiang, P. Heinman and F.J. Himpsel, Phys Rev. Lett. **45** (1980) p.656.

[27] Z.H. Lu and M.J. Graham, Phys. Rev. B **48** (1993) p.4604.

[28] H. Sugahara, M. Oshima, R. Klauser, H. Oigawa and Y. Nannichi, Surf. Sci. **242** (1991) p.335.

[29] A.D. Katanani, H.W. Sang, Jr., P. Chiaradia, and R.S. Baler, L. Vac. Sci. Technol. B **3** (1985) p.608.

[30] W. Rank, J. Finster, and H.J. Kuhr, Surf. Sci. **187** (1987) p.112.

[31] D.K. Biegeslsen, R.D. Briggans, J.E. Northrup and L.E. Swartz, Phys. Rev. Lett. **65** (1990) p.452.

[32] D.J. Chadi, in The structure of surfaces III, Eds. S.Y. Tong, M.A. Van Hove, K. Takayanagi, X.D. Xie (Springer-Verlag, Berlin 1991), p.532.

[33] R. D. Schnell, D. Rieger, A. Bogen, K.W. Wandelt,and W. Steinmann, Solid State Commun. **53** (1985) p.205.

[34] D.A. Woolf, D.I. Westwood, and R.H. Williams, Appl. Phys. Lett. **62** (1993) p.1370.

[34] F. Maeda, Y. Wantanabe, T. Scimeca and M. Oshima, Phys. Rev. B **48** (1993) p.4956.

[35] O. Kubaschewski and C.B Alcock, Metallurgical Thermochemistry, 5th ed. (pergamon, New York, 1979).

[36] E. Yablonovitch, B.J. Skromme, R. Bhat, J. P. Harbison and .J. Gmitter, Appl. Phys. Lett. **54** (1989)p.555.

Chapter 6 Conclusion.

6.1 Summary of Work.

The electronic properties of the InP(100) surface have been characterised for untreated InP and for wet chemically etched InP. The aqueous treatments used in this work were successful in reducing the density of interface states for InP. It was also possible to manufacture reproducible Schottky barrier diodes with reasonable barrier heights and good ideality. Investigations into the effect of anneal temperature on S-InP revealed that increasing anneal temperature encouraged the sulphur to react with the InP improving rectification properties and that at elevated temperatures (870K) the sulphur migrated into the InP bulk completely altering its electronic properties.

Angle resolved ultra-violet photoelectron spectroscopy carried out on the GaAs(111)B surface allowed a preliminary study of the band structure of this surface to be made. The results from this study indicate that there are states in the band gap of GaAs(111)B. The associated study of the effects of molecular sulphur deposition on this surface indicate that sulphur deposition leaves a disordered sulphur top layer but that the underlying As atoms keep a (1x1) periodicity. In comparing the two sets of band structure plots it would appear that the sulphur deposition removes one of the electronic states found on the clean GaAs surface.

Surface sensitive synchrotron core level photoemission studies of the adsorption of molecular sulphur on the clean GaAs(111) surfaces indicate that the sulphur reacts with the topmost atomic layers altering the electronic structure and chemical environment of the atoms. The termination of the (111)A surface by sulphur gallium bonds while not completely removing band bending may reduce the density of surface states. This study also shows that the (111)B surface is not ideally terminated by a sulphur monolayer and is not electronically passivated by sulphur desorption. It can be concluded from the work carried out that it is not possible to simultaneously achieve chemical and electronic passivation by sulphur treatment of the GaAs(111)A or (111)B surface.

6.2 Suggestions for Future work.

There are many directions in which this work could be continued. The sulphur passivated InP surface could be investigated using scanning tunnelling microscope studies, some work has been carried out already in this area [1] but not on the successful etch technique used in this

work. A photoemission study would be very informative revealing valuable information about the chemical properties of sulphur treated InP(100). Further detailed LEED and Auger studies could also be valuable. Also it would be very interesting to carry out a similar study using molecular sulphur in UHV conditions.

Both the angle resolved and core level studies open up avenues for further study. It would be extremely revealing to carry out a similar ARUPS study on the GaAs(111)A surface so that the clean and sulphur treated band structures of both surfaces could be compared. Similar core levels studies of the effect of sulphur deposition were carried out on the various (100) reconstructions at the time of this work. These core level studies could be followed up by putting down selenium on the GaAs surfaces. This could be achieved using a similar electrochemical cell to the one used in this work. The whole area of the interaction of group VI elements with III-V semiconductors could have significant importance in the area of hetrostructural growth.

References

[1] K. Kurihara, Y Miyamoto and K. Furuya, Jpn. J. Appl. Phys. **32** (1993) p.L444-L446.